Plasticity of Cellular Metals (Foams)

Thomas Daxner

Abstract Cellular metals, e.g., made by solidification of molten metal foam, have interesting mechanical properties, among them high specific strength and stiffness coupled with inflammability and good damping properties. This makes them interesting for engineering applications which require the prediction of the onset of yielding under multi-axial stress states and the development of plastic strains over a strain range that may extend into the regime of full compaction of the foam micro-structure, as it is the case in applications for crash protection. This chapter investigates the micro-mechanical deformation mechanisms which govern the elasto-plastic behavior of cellular metals on the macro-mechanical level, where the cellular structure can be treated as a homogeneous material if the difference between the cell size and the component size is large enough. If this is the case suitable constitutive models can be applied for predicting the onset of macroscopic yielding, the evolution of plastic strains and the hardening behavior. Thus, a review of the most important material models proposed for simulating the effective elasto-plastic behavior of isotropic cellular metals is presented. This behavior is characterized by a distinct pressure sensitivity, which sets apart the behavior of cellular metals from the one of solid metals as described by classical (e.g., von Mises) theory of plasticity.

Keywords Cellular metal · Metal foam · Open-cell foam · Closed-cell foam · Yield surface · Flow rule · Hardening · Micromechanics · Multi-axial loading · Pressure dependent yielding

T. Daxner (✉)
CAE Simulation & Solutions, Pitkagasse 2/1/16, A-1210 Vienna, Austria
e-mail: daxner@cae-sim-sol.at

H. Altenbach and A. Öchsner (eds.), *Plasticity of Pressure-Sensitive Materials*,
Engineering Materials, DOI: 10.1007/978-3-642-40945-5_3,

1 Introduction

Cellular metals are a class of materials which is characterized by a foam or sponge-like structure on a length-scale that is typically much smaller than the one of the component. Since the individual cells are much smaller than the typical objects containing cellular metals the mechanical behavior of the cellular structure can generally be described in a homogenized manner, and the present chapter tries to give some insight into the available methods and challenges.

Most cellular materials fall into one of the two following categories:

- open-cell foams (sponges),
- closed-cell foams.

The cells, which are either closed or open according to this classification, are typically filled with air, which is a compressible medium. If the metallic structure is treated as a 'material' in the homogenized sense, this fact gives rise to the marked pressure-sensitivity of cellular metals in the plastic range.

The strength of the materials is primarily determined by the mechanical behavior of the metallic structure, especially in the quasi-static range, where the gas can escape from within the cells through missing or ruptured cell walls. In the case of closed-cell foams the metallic structure consists of a network of struts which meet in vertices and are connected by cell walls in a manner that is very similar to that of liquid foams. This is not surprising, because metallic foams are typically produced by cooling down and solidifying a liquid foam made from molten metal.

In the case of open-cell foams, the metallic skeleton does not form closed cells, because the cell walls are missing, either because they broke during the solidification process or because they where removed by subsequent manufacturing processes.

Interesting structures can be obtained by coating a polymer precursor foam with a metallic layer and subsequently removing the precursor structure. This leaves the struts hollow and, in the ideal case, separates two gas filled cavities, namely the one inside and the one between the struts.

No matter how the cellular metals are produced or which topology they exhibit, their effective mechanical response is rooted in the deformation of the cellular structure itself. To take this fact into account, we investigate deformation mechanisms in cellular metals in Sect. 3.

Transferring theoretical results from the structural level, which is characterized by cells with a size range of tenths of millimeters up to several millimeters, to the component level, which is typically much larger, is a process commonly called homogenization. It is one way of obtaining insight into the mechanical behavior of cellular metals under multi-axial loads. The preferred method, however, is to perform appropriate experiments, which go beyond classical uniaxial compression tests and take multiaxial loading conditions into account. These experiments require expensive equipment and special care owing to the fact that applying hydrostatic pressure by a fluid is difficult because the fluid has to be kept from penetrating into the structure. Nevertheless, corresponding experiments have been performed in the past and the

interpretation of their results has lead to the formulation of constitutive laws for the effective mechanical behavior of cellular metals on the macro-mechanical level.

Section 4 reviews the most important contributions in the field of constitutive modeling of cellular metals. The focus is on works which were tailored to metallic foams, which reduces the number of candidate material models to a handful, and allows for a detailed look into their formulation and derivation. Preceding this main body of this study is a brief introduction to the basics of constitutive modeling for elasto-plastic materials, which will be given in the following Sect. 2.

2 Constitutive Modeling: Basics

2.1 Introduction

Before it is possible to deal with the particular phenomena characterizing the elasto-plastic behavior of cellular metals, it is necessary to acquaint oneself with the basics of continuum mechanics of solid materials and the foundations of the theory of plasticity. This section is intended to provide the reader with the knowledge and the mathematical tools necessary for understanding the formulation of the constitutive models for cellular metals which will be presented in later sections.

First, the mathematical notation used in this chapter will be introduced in Sect. 2.2. Next, the concept of stress will be recapitulated in Sect. 2.3. The description of deformation processes in terms of appropriate strain measures will be reviewed in Sect. 2.4. Finally, Sect. 2.5 describes the elements of the theory of plasticity, which provides the foundation for most of the constitutive laws for cellular metals.

2.2 Mathematical Notation

The most important mathematical terms and operations necessary for performing the derivations presented in this chapter will be briefly summarized in the following. The intention is to familiarize the reader with the mathematical notation used throughout this chapter.

The location of a point in space is described by a vector **x** from the origin of the reference system to the point. In order to do actual numerical calculations, the vector has to be related to a coordinate system 1-2-3 for obtaining its coordinates x_1, x_2, and x_3. Only Cartesian coordinate systems are considered here.

The scalar product of two vectors **a** and **b** gives a scalar c, which is the product of the length of vector **a** with the length of the projection of vector **b** onto vector **a**, and vice versa:

$$c = \mathbf{a} \bullet \mathbf{b} \qquad c = a_i\, b_i \qquad \ldots = \sum_{i=1}^{3} a_i\, b_i, \tag{1}$$

where the use of Einstein's summation notation is indicated by the sum sign. The length l of a vector $\mathbf{v}$ can be calculated as $l = \sqrt{\mathbf{v} \bullet \mathbf{v}}$.

In the framework of tensor algebra a vector is equivalent to a first order tensor $\mathbf{x}$. Such a first order tensor $\mathbf{x}$ can be transformed into a new first order tensor $\mathbf{y}$ by applying a second order tensor $\mathbf{A}$ to it. By writing $\mathbf{y} = \mathbf{A}\,\mathbf{x}$ in tensorial notation, we imply the fact that $\mathbf{A}$ represents a linear transformation of $\mathbf{x}$ into $\mathbf{y}$. The coordinates of the second order tensor $\mathbf{A}$ with respect to an orthonormal coordinate system are indicated as $[\mathbf{A}]_{ij}$ or as A_{ij}, respectively. The coordinates y_i of the transformed tensor $\mathbf{y}$ are a linear combination of the coordinates x_j of the original tensor $\mathbf{x}$, where each original coordinate is weighted by the coordinate A_{ij} of the tensor $\mathbf{A}$. Using both tensor notation and index notation, we obtain

$$\mathbf{y} = \mathbf{A}\,\mathbf{x} \qquad y_i = A_{ij} x_j \qquad \ldots = \sum_{j=1}^{3} A_{ij} x_j. \tag{2}$$

A special second order tensor is the unit tensor $\mathbf{I}$ which has the coordinates $[\mathbf{I}]_{ij} = \delta_{ij}$, where δ_{ij} is the Kronecker Delta function which returns one for $i = j$ and zero for $i \neq j$. Applying the unit tensor to a second order tensor $\mathbf{A}$ leaves the latter tensor unchanged: $\mathbf{I}\mathbf{A} = \mathbf{A}$.

A second order tensor $\mathbf{C}$ can be constructed from vectors $\mathbf{a}$ and $\mathbf{b}$ using the tensor, or dyadic product:

$$\mathbf{C} = \mathbf{a} \otimes \mathbf{b} \qquad C_{ij} = a_i\, b_j \tag{3}$$

The resulting tensor $\mathbf{C}$, applied to a vector $\mathbf{x}$, returns as the result the first vector $\mathbf{a}$, scaled by the product of the length of the second vector $\mathbf{b}$ times the length of the projection of the vector $\mathbf{x}$ onto the second vector $\mathbf{b}$, $(\mathbf{a} \otimes \mathbf{b})\mathbf{x} = \mathbf{a}(\mathbf{b} \bullet \mathbf{x})$.

A second-order tensor $\mathbf{C}$ which represents a transformation $\mathbf{B}$ followed by a transformation $\mathbf{A}$ can be constructed as follows:

$$\mathbf{C} = \mathbf{A}\mathbf{B} \qquad C_{ij} = A_{ik} B_{kj} \qquad \ldots = \sum_{k=1}^{3} A_{ik} B_{kj} \tag{4}$$

A fourth order tensor $\mathbb{C}$ represents a linear transformation which is applied to a second order tensor $\mathbf{A}$ for obtaining a new second order tensor $\mathbf{B}$. We express this operation in tensor notation and index notation:

$$\mathbf{B} = \mathbb{C}\,\mathbf{A} \qquad B_{ij} = C_{ijkl} A_{kl} \qquad \ldots = \sum_{k=1}^{3} \sum_{l=1}^{3} C_{ijkl} A_{kl} \tag{5}$$

The coordinates of the fourth order tensor $\mathbb{C}$ are represented as either $[\mathbb{C}]_{ijkl}$ or C_{ijkl}.

Summing over two indices as in Eq. (5) is called double contraction. The double contraction of a second order tensor $\mathbf{A}$ and another second order tensor $\mathbf{B}$ gives a scalar c. This operation is written as follows:

$$c = \mathbf{A}{:}\mathbf{B} \qquad c = A_{ij}B_{ij} \qquad \ldots = \sum_{i=1}^{3}\sum_{j=1}^{3} A_{ij}B_{ij} \tag{6}$$

The *trace* tr ($\mathbf{A}$) of a second order tensor $\mathbf{A}$ is defined as the sum of the coordinates A_{ii} ($i = 1 \ldots 3$) on the main diagonal (in matrix notation), or the double contraction with the second order tensor of unity $\mathbf{I}$:

$$\text{tr}\,(\mathbf{A}) = \sum_{i=1}^{3} A_{ii} = \mathbf{A}{:}\mathbf{I} \tag{7}$$

The derivative of a scalar-valued function

$$g(\boldsymbol{\sigma}) = g(\sigma_{11}, \sigma_{22}, \sigma_{33}, \sigma_{12}, \sigma_{21}, \sigma_{23}, \sigma_{32}, \sigma_{13}, \sigma_{31})$$

of a second-order tensor $\boldsymbol{\sigma}$ with respect to (the coordinates of) the tensor $\boldsymbol{\sigma}$ gives the gradient of g at $\boldsymbol{\sigma}$, which is itself a second order tensor:

$$\left[\frac{\partial g}{\partial \boldsymbol{\sigma}}\right]_{ij} = \frac{\partial g}{\partial \sigma_{ij}} \tag{8}$$

If the function $g(\boldsymbol{\sigma})$ is homogeneous of degree n in $\boldsymbol{\sigma}$, i.e.,

$$g(\alpha\boldsymbol{\sigma}) = \alpha^n\, g(\boldsymbol{\sigma}) \tag{9}$$

then Euler's theorem on homogeneous functions can be applied to obtain the relationship

$$\frac{1}{g}\boldsymbol{\sigma}{:}\frac{\partial g}{\partial \boldsymbol{\sigma}} = n \qquad \frac{\sigma_{ij}}{g}\frac{\partial g}{\partial \sigma_{ij}} = n \tag{10}$$

which can be useful for manipulating expressions related to plastic flow rules (as introduced in Sect. 2.5).

2.3 The Stress State

In this section, expressions and relationships from continuum mechanics, which are necessary for the mathematical description of the mechanical behavior of materials, are introduced.

The local stress conditions in a body are described by a symmetric second-order tensor $\boldsymbol{\sigma} = [\sigma_{ij}]$ called the stress tensor. The 3/D stress tensor has nine coordinates σ_{ij}, $i \in [1, 3], j \in [1, 3]$, six of which are independent owing to the symmetry of the tensor, i.e., $\sigma_{ji} = \sigma_{ij}$.

Coordinates with identical indices $i = j$ relate to normal loading with respect to the reference coordinate system, whereas coordinates with differing indices $i \neq j$ indicate shear loading.

The actual values of the coordinates of the stress tensor depend on the chosen reference coordinate system. However, three scalar properties I_1, I_2, and I_3, can be defined which are invariant with respect to a rotation of the reference system, These invariants are given by:

$$I_1 = \sigma_{kk} = \sigma_{11} + \sigma_{22} + \sigma_{33} \tag{11}$$

$$I_2 = \frac{1}{2}\left(\sigma_{ii}\sigma_{kk} - \sigma_{ij}\sigma_{ij}\right) \tag{12}$$

$$I_3 = \det \boldsymbol{\sigma} \tag{13}$$

It is possible to find a reference frame 1-2-3 for which all non-diagonal coordinates of the stress tensor, i.e., the shear stresses, vanish. The coordinates σ_{ii} along the diagonal of the stress tensor expressed in this specific reference system are then called the principal stresses, $\sigma_1 = \sigma_{11}$, $\sigma_2 = \sigma_{22}$, and $\sigma_3 = \sigma_{33}$. They are the eigenvalues of the stress tensor and can be found by solving the characteristic equation

$$\det(\boldsymbol{\sigma} - \sigma_i \mathbf{I}) = -\sigma_i^3 + I_1\,\sigma_i^2 - I_2\,\sigma_i + I_3 = 0. \tag{14}$$

For the investigation of the mechanical behavior of pressure sensitive materials, it is necessary to define the pressure p, which is a function of the normal stresses only:

$$p = -\frac{1}{3}\left(\sigma_{11} + \sigma_{22} + \sigma_{33}\right) = -\sigma_{\mathrm{m}} \tag{15}$$

Also defined in Eq. (15) is the mean stress σ_{m}, which has the negative value of the pressure, $\sigma_{\mathrm{m}} = -p$. Note the relationship $\sigma_{\mathrm{m}} = \frac{1}{3} I_1$ between the mean stress and the first invariant I_1 of the stress tensor, compare Eq. (11).

The contribution of the hydrostatic pressure to the stress tensor can be isolated as

$$\boldsymbol{\sigma}_{\mathrm{Hydro}} = -p\,\mathbf{I} = \sigma_{\mathrm{m}}\,\mathbf{I} \tag{16}$$

Correspondingly, the deviatoric part $\mathbf{s}$ of the stress tensor can be obtained by subtracting the hydrostatic part from the stress tensor,

$$\mathbf{s} = \boldsymbol{\sigma} - \boldsymbol{\sigma}_{\mathrm{Hydro}} \qquad \ldots = \boldsymbol{\sigma} - \sigma_{\mathrm{m}}\,\mathbf{I} = \boldsymbol{\sigma} + p\,\mathbf{I} \tag{17}$$

For the deviatoric stress tensor $\mathbf{s}$ three invariants J_1, J_2, and J_3 can be defined. The first invariant J_1 is zero by definition, because the deviatoric stress tensor contains no contribution from hydrostatic pressure. The second invariant J_2 is given by

$$J_2 = \frac{1}{2}\mathbf{s}{:}\mathbf{s} = \frac{1}{2}s_{ij}s_{ij}$$

It plays an important role in metal plasticity, since it can be used to express the von Mises equivalent stress σ_e in the following form:

$$\sigma_\mathrm{e} = \sqrt{3J_2} \quad \ldots = \sqrt{\frac{3}{2}\mathbf{s}{:}\mathbf{s}}. \tag{18}$$

For some materials, in particular metals, which are not sensitive to pressure with regard to yielding, the von Mises equivalent stress is an appropriate scalar measure for assessing the stress state in the material with respect to plastic yielding. For uniaxial tension and compression, the von Mises stress is equal to the applied stress. It is sometimes useful to re-write the von Mises stress in terms of principal stresses:

$$\sigma_\mathrm{e} = \sqrt{\frac{1}{2}\left[(\sigma_1-\sigma_2)^2 + (\sigma_2-\sigma_3)^2 + (\sigma_3-\sigma_1)^2\right]} \tag{19}$$

At this point, some partial derivatives of scalar-valued functions of the stress tensor with respect to the stress tensor coordinates, recall Eq. (8), are presented in Table 1.

Table 1 Some useful derivatives of quantities related to the description of yield surfaces for pressure-sensitive materials with respect to the coordinates σ_{ij} of the stress tensor $\boldsymbol{\sigma}$

Tensor notation of derivative	Selected terms in index notation
$\frac{\partial(\mathbf{s}:\mathbf{s})}{\partial\boldsymbol{\sigma}} = 2\mathbf{s}$	$\frac{\partial(s_{ij}s_{ij})}{\partial\sigma_{11}} = 2\left(\sigma_{11} - \frac{\sigma_{11}+\sigma_{22}+\sigma_{33}}{3}\right) = 2s_{11}$
	$\frac{\partial(s_{ij}s_{ij})}{\partial\sigma_{12}} = 2\sigma_{12} = 2s_{12}$
$\frac{\partial\sigma_\mathrm{e}}{\partial\boldsymbol{\sigma}} = \frac{3}{2}\frac{\mathbf{s}}{\sigma_\mathrm{e}}$	$\frac{\partial\sigma_\mathrm{e}}{\partial\sigma_{11}} = \frac{1}{2\sigma_\mathrm{e}}\left[2\sigma_{11}-\sigma_{22}-\sigma_{33}\right] = \frac{3s_{11}}{2\sigma_\mathrm{e}}$
	$\frac{\partial\sigma_\mathrm{e}}{\partial\sigma_{12}} = \frac{3\sigma_{12}}{2\sigma_\mathrm{e}}$
$\frac{\partial(\sigma_\mathrm{e}^2)}{\partial\boldsymbol{\sigma}} = 3\mathbf{s}$	$\frac{\partial(\sigma_\mathrm{e}^2)}{\partial\sigma_{11}} = 2\sigma_{11}-\sigma_{22}-\sigma_{33} = 3s_{11}$
	$\frac{\partial(\sigma_\mathrm{e}^2)}{\partial\sigma_{12}} = 3\sigma_{12} = 3s_{12}$
$\frac{\partial\sigma_\mathrm{m}}{\partial\boldsymbol{\sigma}} = \frac{1}{3}\mathbf{I}$	$\frac{\partial\sigma_\mathrm{m}}{\partial\sigma_{11}} = \frac{1}{3}$
$\frac{\partial(\sigma_\mathrm{m}^2)}{\partial\boldsymbol{\sigma}} = \frac{2}{3}\sigma_\mathrm{m}\,\mathbf{I}$	$\frac{\partial(\sigma_\mathrm{m}^2)}{\partial\sigma_{11}} = \frac{2}{9}\left[\sigma_{11}+\sigma_{22}+\sigma_{33}\right]$
$\frac{\partial p}{\partial\boldsymbol{\sigma}} = -\frac{1}{3}\mathbf{I}$	$\frac{\partial p}{\partial\sigma_{11}} = -\frac{1}{3}$
$\frac{\partial(p^2)}{\partial\boldsymbol{\sigma}} = -\frac{2}{3}p\,\mathbf{I}$	$\frac{\partial(p^2)}{\partial\sigma_{11}} = \frac{2}{9}\left[\sigma_{11}+\sigma_{22}+\sigma_{33}\right]$

Left column: tensor notation, right column: selected terms in index notation

Materials, for which the mechanical response is independent of any material direction, are called isotropic materials. Since the choice of the reference coordinate system for the description of the constitutive behavior of these materials is not predetermined by any geometrical feature that introduces a direction dependency (such as fibers in a fiber-reinforced composite material) it is possible to describe the material behavior in terms of tensor invariants, and, in particular, in terms of the three principal stresses.

The yield surface, which plays a major role in any plasticity model (compare Sect. 4), is often depicted in the three-dimensional space that is described by interpreting the three principal stresses σ_1, σ_2, and σ_3 as coordinates in an orthonormal reference system. In this principal stress space, the following interesting entities can be identified:

Hydrostatic axis:	The space diagonal in the principal stress space, describing stress states that are purely hydrostatic and do not contain any deviatoric component, i.e., $\sigma_e = 0$.
Deviatoric plane:	Any plane perpendicular to the hydrostatic axis, i.e., all stress states with the same mean stress $\sigma_m = \text{const}$.
π-plane:	The deviatoric plane which contains the origin $\sigma_1 = \sigma_2 = \sigma_3 = 0$ of the principal stress coordinate system, and, therefore, all stress states with vanishing mean stress, $\sigma_m = 0$.
Meridian:	A plane which contains the hydrostatic axis.

Most of the constitutive laws for the description of the effective mechanical behavior of isotropic cellular metals can be formulated in terms of the mean stress σ_m and the von Mises equivalent stress σ_e. Surfaces in the principal stress space, which are defined implicitly by $F(\sigma_m, \sigma_e) = 0$ show rotational symmetry about the hydrostatic axis.

If this rotational symmetry cannot be assumed, a third parameter in addition to σ_m and σ_e has to be considered. This third parameter is often chosen to be an angle θ measured in the π-plane, namely between the projection of the σ_1-axis on the π-plane and a vector from the origin of the principal stress space to the projection of the stress state onto the π-plane along the direction of the hydrostatic axis. By this geometrical definition, the angle θ, which is often called the Lode angle, can assume values between 0 and 60°, provided that the principal stresses are sorted as $\sigma_1 \geq \sigma_2 \geq \sigma_3$. The Lode angle can be calculated from

$$\cos 3\theta = \frac{3\sqrt{3}}{2} \frac{J_3}{\sqrt{(J_2)^3}} \tag{20}$$

Note the dependency of this quantity on the third invariant J_3 of the stress deviator tensor. For purely hydrostatic stress states, θ becomes undefined, because inserting $J_2 = 0$ in Eq. (20) would cause a division by zero. The Lode angle describes the relationship between the principal stresses.

2.4 Deformation and Strain

Application of loads to solid bodies leads to a deformation of these bodies. The quantities and methods available for the description of this deformation are the topics of this section.

We investigate a process, which moves and deforms a body from an undeformed reference configuration to a deformed configuration. Points $\mathbf{X}$ in the undeformed configuration are mapped onto points in the deformed configuration by the function $\boldsymbol{\varphi}$, giving $\mathbf{x} = \boldsymbol{\varphi}(\mathbf{X}, t)$ at any given time t.

Correspondingly, a line element $d\mathbf{X}$ in the undeformed configuration is transformed into a line element in the actual configuration $d\mathbf{x}$ according to $d\mathbf{x} = \mathbf{F}\, d\mathbf{X}$, where $\mathbf{F}$ is a second order tensor called the deformation gradient, and is defined as

$$\mathbf{F} = \frac{\partial \boldsymbol{\varphi}}{\partial \mathbf{X}} \qquad F_{ij} = \frac{\partial \varphi_i}{\partial X_j} \tag{21}$$

The deformation gradient $\mathbf{F}$ contains all the necessary information for describing the deformation process at a given material point. In particular, it contains information about the actual deformation of the material and any super-imposed rigid body rotation. To separate these two contributions, a polar decomposition of $\mathbf{F}$ into an orthogonal rotation tensor $\mathbf{R}$ (with properties $\det(\mathbf{R}) = 1$, $\mathbf{R}^{\mathrm{T}} = \mathbf{R}^{-1}$) and a symmetric tensor $\mathbf{U}$, which is called the right (or material) stretch tensor, can be performed:

$$\mathbf{F} = \mathbf{R}\mathbf{U} \tag{22}$$

This decomposition means that the shape and/or volume of a volume element dV is first changed according to $\mathbf{U}$ and the volume element is then rotated by $\mathbf{R}$ into the final configuration dv. The three eigenvalues λ_i of $\mathbf{U}$ are called the principal stretches. The length of a line element dL_i in the undeformed configuration, which points into the direction of the i-th eigenvector $\mathbf{N}_i$ of $\mathbf{U}$ is stretched by the deformation process to a new length dl_i, which can be calculated using

$$\lambda_i = \frac{dl_i}{dL_i} \tag{23}$$

To actually calculate the right stretch tensor $\mathbf{U}$, we first introduce the right Cauchy-Green tensor $\mathbf{C}$:

$$\mathbf{C} = \mathbf{F}^{\mathrm{T}}\mathbf{F} = \mathbf{U}^{\mathrm{T}} \underbrace{\mathbf{R}^{\mathrm{T}}\mathbf{R}}_{\mathbf{I}} \mathbf{U} = \mathbf{U}^{\mathrm{T}}\mathbf{U} \tag{24}$$

This tensor has the eigenvalues Λ_i and the eigenvectors $\mathbf{N}_i$, and can be represented using the spectral decomposition theorem:

$$\mathbf{C} = \sum_{i=1}^{3} \Lambda_i \mathbf{N}_i \otimes \mathbf{N}_i \tag{25}$$

We can now build the right stretch tensor $\mathbf{U}$ in a similar manner noting that it has the same eigenvectors as $\mathbf{C}$ and its eigenvalues λ_i are the square root of the eigenvalues Λ_i of $\mathbf{C}$, i.e., $\lambda_i = \sqrt{\Lambda_i}$:

$$\mathbf{U} = \sum_{i=1}^{3} \lambda_i \mathbf{N}_i \otimes \mathbf{N}_i \tag{26}$$

The principal stretches already give a lot of information about the deformation process, but they do not lend themselves naturally to the description of the strain in the material, because they assume a value of one for the undeformed state (for which, in the absence of residual stresses, the stresses are zero).

Therefore, appropriate strain measures have to be defined. For large deformations, logarithmic strain measures are often used. The logarithmic strain tensor in the reference configuration is defined as

$$\boldsymbol{\varepsilon} = \sum_{i=1}^{3} \ln(\lambda_i) \mathbf{N}_i \otimes \mathbf{N}_i \tag{27}$$

For homogenous uniaxial deformations, the axial logarithmic strain can be found as $\varepsilon_{\text{axial}}^{(\ln)} = \ln(l/l_0) = \ln(\lambda_{\text{axial}})$. It is zero for the undeformed state.

It is often useful to split the strain tensor into a part which describes the change of shape of a volume element and a part which describes the change of its volume.

Let us look at a cube-shaped volume element dV which is oriented along the eigenvectors $\mathbf{N}_i$. The undeformed edge length is given by dL, and the undeformed volume by $dV = dL^3$. If the volume element is transformed into the deformed configuration by the right stretch tensor $\mathbf{U}$, its edges remain orthogonal (because they where parallel to the eigenvectors of $\mathbf{U}$) but their length is now dl_1, dl_2, and dl_3, respectively. The volume in the deformed configuration is, thus, $dv = dl_1 dl_2 dl_3$. Relating the deformed volume dv to the undeformed volume dV, we can now define the logarithmic volumetric strain ε_{vol}:

$$\begin{aligned} \varepsilon_{\text{vol}} &= \ln \frac{dv}{dV} = \ln \frac{dl_1 dl_2 dl_3}{dL^3} = \ln(\lambda_1 \lambda_2 \lambda_3) = \ln(\lambda_1) + \ln(\lambda_2) + \ln(\lambda_3) \\ &= \varepsilon_1^{(\ln)} + \varepsilon_2^{(\ln)} + \varepsilon_3^{(\ln)} \end{aligned} \tag{28}$$

This shows the convenient property that the logarithmic volumetric strain is equal to the trace of the logarithmic strain tensor $\boldsymbol{\varepsilon}$.

The part of the strain tensor, which changes the volume of a volume element can now be isolated as: $\boldsymbol{\varepsilon}_{\text{vol}} = \frac{1}{3}\varepsilon_{\text{vol}}\mathbf{I}$. The remaining, deviatoric part $\mathbf{e}$ of strain tensor can be found by subtracting this tensor from the full strain tensor:

$$\mathbf{e} = \boldsymbol{\varepsilon} - \boldsymbol{\varepsilon}_{\mathrm{vol}} = \boldsymbol{\varepsilon} - \frac{1}{3}\varepsilon_{\mathrm{vol}}\mathbf{I} \tag{29}$$

Since the deviatoric strain tensor does not impose any volume change, its trace is equal to zero.

Similar to the von Mises equivalent stress σ_{e}, an equivalent or effective strain ε_{e} can be defined from the deviatoric part of the strain tensor:

$$\varepsilon_{\mathrm{e}} = \sqrt{\frac{2}{3}\mathbf{e}:\mathbf{e}} \tag{30}$$

This definition implies two properties: (a) for a volume-preserving uniform extension process, the effective strain is equal to the axial strain, and (b) the effective strain is work conjugate to the von Mises equivalent stress σ_{e}.

In addition, the rate $\dot{\varepsilon}_{\mathrm{vol}}$ of the logarithmic volumetric strain is work conjugate to the mean stress σ_{m}. Finally, an expression for the rate $\dot{W}$ of the internal mechanical work done by the stresses can be obtained exclusively in terms of effective properties:

$$\dot{W} = \sigma_{\mathrm{e}}\dot{\varepsilon}_{\mathrm{e}} + \sigma_{\mathrm{m}}\dot{\varepsilon}_{\mathrm{vol}} \tag{31}$$

2.5 Formal Introduction to Elasto-Plasticity

In this section, the common framework of the constitutive modeling of elastic-plastic materials will be reviewed.

A solid body under global loading experiences local stress fields in parts or all of its volume. These stresses lead to deformations, which can be expressed by strain tensors on the material point level. The local deformation state is described by a strain tensor $\boldsymbol{\varepsilon}$.

The strain state is related to the stress state by constitutive laws, which express the strain tensor $\boldsymbol{\varepsilon}$ in terms of the stress tensor $\boldsymbol{\sigma}$, the temperature T (if necessary), and internal variables S_i:

$$\boldsymbol{\varepsilon} = f(\boldsymbol{\sigma}, T, S_i) \tag{32}$$

The internal variables S_i describe the internal state of the material. Accumulated plastic strains, e.g., are important internal variables for plasticity. The description of the evolution of the material state throughout the deformation process requires evolution equations for the internal variables:

$$\frac{\mathrm{d}S_i}{\mathrm{d}t} = g_i(\boldsymbol{\sigma}, T, S_i) \tag{33}$$

The coupled system of Eqs. (32) and (33) has to be solved in order to obtain the deformation history of the material.

We now consider materials which deform inelastically, i.e., which are able to undergo irreversible, plastic deformations. These material often do not show yielding from the onset, but rather require a certain yield stress state to be exceeded before plastic deformation sets in. If the stress state is not critical with respect to plastic yielding, the material deforms elastically.

Classical plasticity theory (see e.g. [26]) describes this behavior by defining a surface in stress space the interior of which contains all stress states for which the deformation mechanism remains purely elastic. This surface is called yield surface. The yield surface is defined implicitly by the relationship

$$F(\boldsymbol{\sigma}, S_i, T) = 0 \tag{34}$$

where F is called the yield function. The interior of the yield surface contains all material states for which $F < 0$.

As soon as stress states reach the yield surface, and, consequently, the yield criterion $F(\boldsymbol{\sigma}, S_i) = 0$ is fulfilled, the material starts accumulating plastic strains $\boldsymbol{\varepsilon}_{\mathrm{pl}}$ at a rate, which is defined by the plastic *flow rule* (given here in incremental form):

$$d\boldsymbol{\varepsilon}_{\mathrm{pl}} = d\boldsymbol{\varepsilon}_{\mathrm{pl}}(\boldsymbol{\sigma}, d\boldsymbol{\sigma}, S_i, T). \tag{35}$$

The flow rule is often defined using the gradient of a flow potential $G(\boldsymbol{\sigma}, S_i, T)$:

$$d\boldsymbol{\varepsilon}_{ij}^{(\mathrm{pl})} = d\lambda \, \frac{\partial G}{\partial \sigma_{ij}} \tag{36}$$

Herein, $d\lambda$ is the increment of the plastic flow multiplier λ, which can be determined using the fact that the stress state always fulfills the yield condition (34) during plastic loading. By definition, the stress state always remains on the yield surface as long as the material point deforms plastically.

The size, the location and the shape of the yield surface, however, can change according to the applied constitutive theory. The evolution of the yield surface is described by the evolution laws for the relevant internal variables S_i, e.g., by appropriate *hardening laws*.

For many constitutive laws, the flow potential G is chosen to be identical to the yield function, $G \equiv F$. The corresponding flow rules are called *associated* flow rules.

In a general deformation process involving plastic deformation, contributions from elastic deformation mechanisms and plastic yielding are superimposed. If the elastic deformations remain small compared to the overall deformations, an additive split of the strain tensor $\boldsymbol{\varepsilon}$ into an elastic part $\boldsymbol{\varepsilon}_{\mathrm{el}}$ and a plastic part $\boldsymbol{\varepsilon}_{\mathrm{pl}}$ is appropriate:

$$\boldsymbol{\varepsilon} = \boldsymbol{\varepsilon}_{\mathrm{el}} + \boldsymbol{\varepsilon}_{\mathrm{pl}} \tag{37}$$

3 Deformation Mechanisms and Yielding in Cellular Metals

3.1 Onset of Failure

While cellular metals can be treated as homogeneous materials for most applications because of the size difference between their metallic structure and the size of corresponding components, their mechanical behavior is still governed by deformation mechanisms in the metallic structure itself.

For open-cell metallic foams, the bending and buckling of the struts is the dominating deformation mechanism. Usually, the struts of open-cell foams have two distinct geometrical properties:

- their cross-sections have the shapes of triangles with concave sides, which is a result of surface tension and drainage processes acting on the foam structure as long as it is in a molten state. The characteristic shape of these struts is called a Plateau border. Figure 1 shows the struts enclosing a single open cell.
- The cross-sectional area of the struts is smallest around their middle and increases towards the vertices. This means that the vertices are considerably stiffer than the struts and, consequently, rather rotate and move than deform.

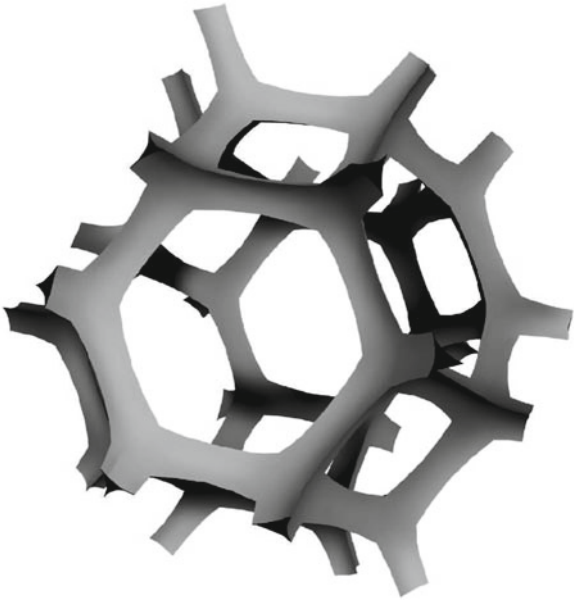

Fig. 1 Rendering of the Plateau border network forming the structure of an open-cell foam. Adapted from [2]

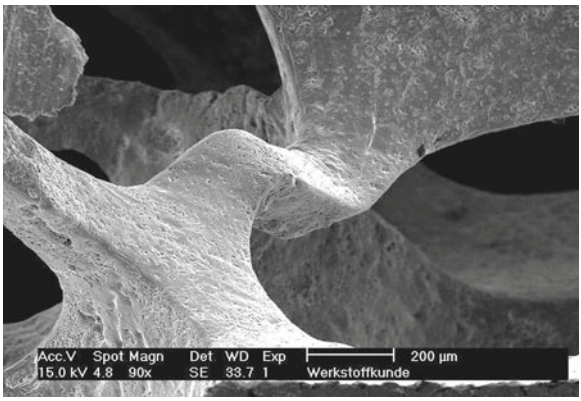

Fig. 2 Local bending deformation of a strut in an open-cell metal foam (image courtesy of Institute of Materials Science and Testing, Vienna University of Technology)

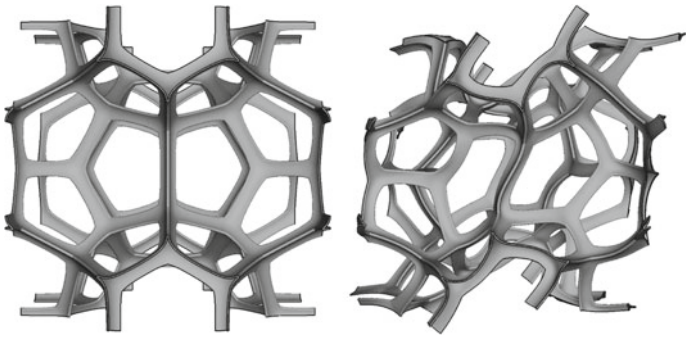

Fig. 3 Buckling of an open-cell structure with hollow struts under hydrostatic pressure

Struts in open-cell materials experience normal loads, bending moments, and torsional loads depending on the macromechanical loading conditions, their orientation and their connection to the surrounding framework of struts.

Figure 2 shows a typical deformation mode of a strut in an open-cell metallic foam. The deformation pattern can be the result of bending by transverse forces or moments, or elasto-plastic buckling. It is obvious that the deformation affects mainly the thin middle section of the struts whereas the thick vertices perform rigid body movements.

Subjecting regular cellular model structures to macroscopic hydrostatic pressure loading may cause struts to experience compressive stresses which can lead to buckling. This buckling can be global in nature, as is shown in Fig. 3 for a periodic unit cell model of an open-cell structure with hollow struts. In this simulation the periodicity of the buckling mode is tied to the geometrical periodicity of the unit cell. Simulation methods, which can capture buckling modes with wavelengths far exceeding the dimensions of the constituting unit cell model, deserve to be mentioned in this

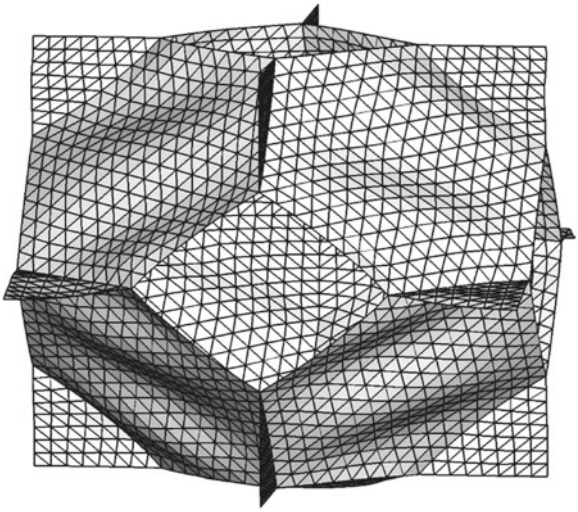

Fig. 4 Cell wall buckling in a unit cell model of a regular tetrakaidecahedral cell structure under macroscopic uniaxial tension

context [19, 20, 25, 32]. Even if the initial buckling mechanism was an elastic one, stress redistribution due to the excentric loading of the struts in the post-buckling regime can quickly lead to plastic yielding in the outer zones of the struts.

For closed-cell foams the presence of cell walls adds the additional mechanisms of bending and stretching of the cell walls. In the direction of compressive principal stresses, the cell walls may buckle, and they may rupture if the local stresses exceed the strength of the walls.

A tetrakaidecahedral unit cell model of a closed-cell foam can be used to illustrate an interesting phenomenon in connection with elastic buckling of cell walls, compare Fig. 4. Here, elastic buckling can be observed on the cell wall level even though the macroscopic loading state is one of uniaxial tension. The reason for this is the fact that the hexagonal faces, which are oblique to the loading direction, experience in-plane shear loading rather than pure tensile loading, causing shear buckling as soon as the critical stress is exceeded.

Micro-mechanical unit cell models can also be exploited to demonstrate the initial stages of deformation in a closed-cell foam under uniaxial compressive loading. Figure 5 shows a uniaxial compressive stress versus compressive strain diagram for a periodic tetradecahedral unit cell model. A straight line at the beginning of the stress-strain curve represents the regime of linear elastic deformation. It is not completely clear, if such a distinct linear regime exists in a real cellular metal owing to the fact that such a material usually contains many imperfections and inhomogeneities that can trigger plastic yielding under even the slightest macroscopic load.

As the macroscopic load is increased, the stresses inside the cellular structure rise and, inevitably, reach the yield stress of the solid material in the first critical spots.

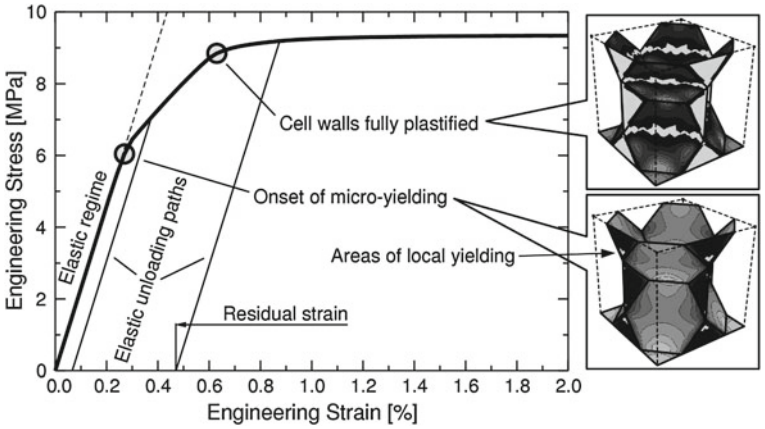

Fig. 5 Compressive stress versus strain diagram for the uniaxial compression of a regular, periodic tetrakaidecahedral cellular structure. The two small contour plots on the right side show the distributions of the von Mises equivalent stress at the onset of local yielding (*bottom*) and close to the limit stress (*top*) (from [9])

These spots are indicated by an arrow in Fig. 5, and they mark the influence regions of stress concentrations in the vicinity of the vertices of the model structure. After the initiation of yielding the stress-strain-curve starts to deviate visibly from the tangent in the origin of the stress versus strain curve. Elastic unloading beyond the onset of micro-yielding can be simulated for obtaining the residual plastic strains in the structure as is also shown in Fig. 5.

Because the detection of micro yielding as defined by the determination of the onset of yielding in any integration point or finite element node in the simulation model may be mesh-dependent or predict yielding at stresses much lower than the macroscopic yield stress, it can prove advantageous to define yielding based on the magnitude of the macroscopic plastic strain which remains after the structure has been unloaded, similar to the definition of the offset yield point for metals without a distinct elastic limit stress.

As the compressive load increases, larger and larger sections of the cell walls start to deform plastically. Finally, as the plastic deformation bands in the cell walls connect across the individual cells, the limit load of the unit cell model is nearly reached and the compressive stress-strain-curve shows a nearly horizontal plateau.

Even though a fairly simple finite element unit cell model was used for obtaining Fig. 5, it can nevertheless illustrate the sequence of events leading to plastic failure of cellular metals.

In solid metals the application of hydrostatic pressure does not cause plastic yielding, at least not within the confines of classic metal plasticity theory. In cellular metals, however, applying hydrostatic pressure on the macroscopic level will lead to local stress states in the cellular structure which are—depending on the symmetry and regularity of the structure—predominantly uniaxial and compressive. Thus, they

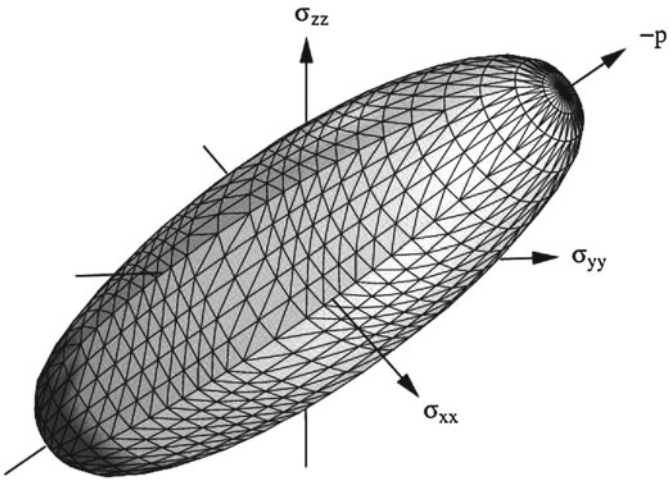

Fig. 6 Yield surface of a regular closed-cell foam predicted by a periodic Weaire-Phelan unit cell model. The dark cap at the end of the ellipsoidal in the regime of positive hydrostatic pressure values indicates stress states, for which yielding may be preceded by elastic buckling (from [10])

can and will cause plastic yielding, because the macroscopic hydrostatic load does not lead to hydrostatic stress states on the micromechanical level.

By loading a sample made of cellular metal along different paths in stress space, stress states for which the macromechanical behavior becomes inelastic can be determined and connected to form a yield surface in the stress space. This can be done experimentally or by means of numerical models.

Figure 6 shows a yield surface in principal stress space that was predicted for a periodic finite element unit cell model of a Weaire-Phelan structure, which is a good generic model for closed-cell foams. In accordance with the statements above, the yield surface intersects the hydrostatic axis at the points corresponding to the hydrostatic tensile and compressive yield stresses. The shape of the yield surface is the one of an ellipsoid which is elongated along the hydrostatic axis.

From a numerical point of view, Fig. 6 contains additional information in the form of the darkened cap at the end of the yield surface which corresponds to almost purely hydrostatic compression. In those dark areas on the yield surface the system matrix has negative eigenvalues, which means that elastic buckling precedes or prematurely initiates plastic yielding.

Figure 6 shows an ellipsoidal yield surface which is visibly elongated along the axis of hydrostatic stress states. This can be attributed to the fact that the stress states induced in the cell walls are mainly membrane-like for hydrostatic loads on the one hand and characterized by high bending stresses close to the vertices for uniaxial loads, on the other hand, which initiates yielding at deviatoric macroscopic stresses that are lower than the hydrostatic macroscopic yield stresses.

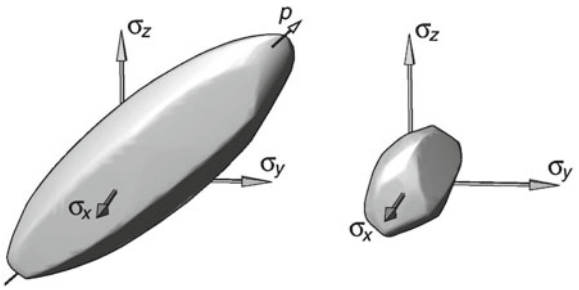

Fig. 7 Yield surfaces predicted for a regular (*left*) and an irregular (*right*) tetrakaidecahedral unit cell model of closed-cell foam, respectively [8]

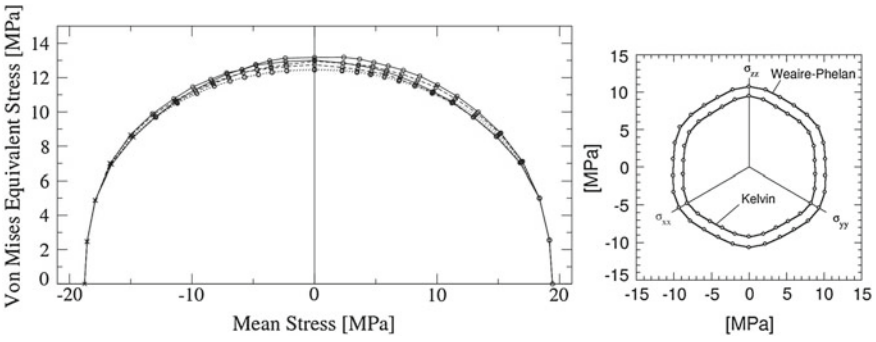

Fig. 8 Projection of the yield surfaces predicted for two periodic unit cell models of closed-cell foam into a diagram of von Mises equivalent stress σ_e versus mean stress σ_m (*left*). Cross-section of the yield surfaces by a deviatoric plane (*right*, from [10])

For real cellular metals, the difference between length and diameter of the ellipsoid is not expected to be so pronounced, as is illustrated in Fig. 7, which presents the yield surface of a regular tetrakaidecahedral finite element unit cell model (left) and the yield surface of a unit cell model with the same topology, but randomly perturbed vertex positions (right). The geometrically imperfect, and therefore more realistic model, shows a smaller yield surface with a much lower ratio between the length and the diameter of the ellipsoidal, which is closer to the experimental evidence. The reason behind this are the bending moments which are induced by excentrical loading of the microstuctural members in the case of the irregular unit cell model even for predominantly hydrostatic macroscopic pressure.

A common method of visualizing yield surfaces of cellular metals is the projection of points on the yield surface onto a diagram of von Mises equivalent stress σ_e versus mean stress σ_m. Figure 8 (left) displays the points on the yield surface in Fig. 6 in the corresponding form. In this diagram, the yield surface collapses into a point cloud which can be fitted by an elliptical curve in a first approximation.

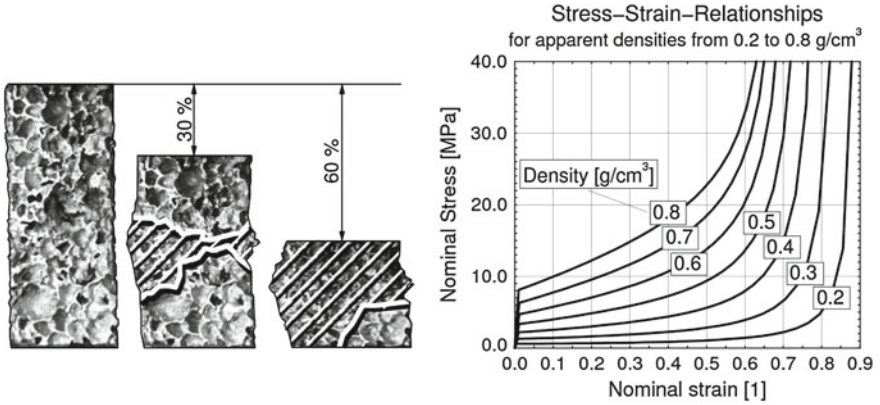

Fig. 9 A sample of a foam specimen in the unloaded state and at 30 and 60 % compressive nominal strain, respectively (*left*). Generic stress versus strain curves for different apparent aluminum foam densities are shown on the right (after [21])

The fact that the points do not sit on a single curve indicates that the yield surface does not have a circular cross-section in any deviatoric plane, $\sigma_m = \text{const}$. Figure 8 (right) shows such a cross section. Consequently, for an exact description of the yield surface, the von Mises equivalent stress σ_e and the mean stress σ_m are not sufficient and an additional measure such as the third invariant J_3 of the deviatoric stress tensor or the Lode angle (20) has to be supplied. Experimental evidence for an influence of the third invariant J_3 on the yield surface shape has been provided by [5, 6, 12].

3.2 Progressive Collapse and Densification

The plateau region of the uniaxial compressive stress-strain relationship is characterized by the successive collapse of layers of cells, starting from the weakest cell layer and spreading either into neighboring regions or other weak layers in different sections of the specimen. This process is indicated by the extent of the hatched regions in Fig. 9 (left) which mark the collapsed regions at two stages of compression of a particular sample of metallic foam. Generally, some amount of hardening can be expected, because the collapsed layers show high resistance to further compression and the remaining uncollapsed regions are stronger than the collapsed ones in their initial state. In addition, the metallic bulk material itself typically experiences strain hardening.

Increasing the load leaves only stiff and strong cells undamaged. In combination with the collapsed cells, which are nearly incompressible in relation to the undamaged ones, this means that the slope of the uniaxial compressive stress-strain relationship is getting steeper and steeper.

Finally, with the application of sufficiently high compressive stresses, all cells along the loading path are expected to collapse. This stage of uniaxial compression is called densification, because it is characterized by most of the void volume being squeezed out of the cellular structure and the mechanisms of the bending and stretching of cell struts and walls being replaced by the transfer of compressive forces along bridges of solid bulk material formed by the structural members of collapsed cells which are in contact with each other.

The following approximation of the nominal compressive densification strain ε_{D} as a linear function of the relative density $\rho_{\mathrm{rel}} = \rho^*/\rho_{\mathrm{S}}$, where ρ^* is the apparent density of the cellular material and ρ_{S} is the density of the bulk material, is suggested in [17]:

$$\varepsilon_{\mathrm{D}} = 1 - 1.4\frac{\rho^*}{\rho_{\mathrm{S}}} \tag{38}$$

The effective uniaxial compressive response of a cellular metal depends on

1. the relative density of the cellular metal,
2. the topology and the homogeneity of the cell structure,
3. the hardening behavior and the ductility of the bulk material.

The influence of the relative density on the effective uniaxial compressive stress-strain behavior was captured in the comprehensive study [21] including a large number of quasi-static compressive tests on Al99.5 foam specimens of varying density.

To express the dependency of the compressive stress-strain response of this particular material on its relative density, an analytical relationship between the nominal stress σ and the nominal strain ε proposed by Shim [31] was fitted to the experimentally obtained stress-strain curves. Below a collapse stress σ_0, and a corresponding collapse strain ε_0, respectively, the uniaxial compressive stress σ is assumed to be a linear function of the compressive strain ε. The plateau region and the densification regime are described by the superposition of a linear and an exponential function of the compressive strain, which are parameterized by shape parameters a, b, ε_0 and n according to the second line of the following equation:

$$\sigma(\varepsilon) = \sigma_0 \begin{cases} \dfrac{\varepsilon}{\varepsilon_0} & : \quad \varepsilon \leq \varepsilon_0 \\ \exp\left(\dfrac{a(\varepsilon - \varepsilon_0)}{(a-\varepsilon)^n}\right) - b(\varepsilon - \varepsilon_0) & : \quad \varepsilon_0 < \varepsilon < a \end{cases} \tag{39}$$

Gradinger [21] derived the following relationships between the curve parameters and the apparent density ρ of the investigated material, which has to be inserted in $\left[\mathrm{g/cm^3}\right]$:

$$
\begin{aligned}
a(\rho) &= -0.37004\rho + 1.0000 \\
b(\rho) &= 6.6964\rho^2 - 10.2790\rho + 2.3053 \\
\varepsilon_0(\rho) &= -0.0459\rho^2 + 0.0563\rho - 0.0055 \\
n(\rho) &= -1.3633\rho^2 + 1.2243\rho + 0.3321 \\
\sigma_0(\rho) &= 12.3430 \times \rho^{1.8807}\ \text{[MPa]}
\end{aligned}
\tag{40}
$$

The corresponding uniaxial compressive stress-strain curves are shown in Fig. 9, right. It is evident that the collapse of low density Al99.5 foam progressed along a long plateau regime of nearly constant compressive stress up to a nominal densification strain of nearly 90 %. In contrast, densification occurred between 60 and 70 % nominal compressive strains for aluminum foams of higher apparent density and the hardening modulus of these foams was considerably higher.

4 Constitutive Modeling of Cellular Metals

4.1 Introduction

Cellular materials have a complicated micro-structure which generally cannot be described in its entirety by testing and visualization methods. Nevertheless, the effective mechanical behavior of the cellular material is a consequence of the interaction of the deformation mechanisms of the countless structural members on the cellular level. Since it is not feasible to model the micro-structure, the mechanical response of the cellular metals has to be described in a macroscopic, averaged-out sense within the framework of the theory of plasticity. This approach requires that the overall dimensions of the structures made of foam are at least one or two orders of magnitude larger than the typical size of typical individual foam cells.

Constitutive laws for cellular metals have to primarily account for the fact that these materials can yield under purely hydrostatic stress states, and, consequently, can acquire volumetric plastic deformations when being loaded beyond the yield limit. This is clearly in contrast with the assumption of classical theory of plasticity for solid metals, that hydrostatic stresses — however high — will not cause plastic deformations, and that plastic flow does not result in changes of the volume.

Consequently, new constitutive laws had to be developed for cellular metals, and these constitutive theories will be the subject of this section. An early overview of constitutive laws for the simulation of metallic foams was compiled by Hanssen et al. [23, 24]. They compare constitutive formulations proposed by Schreyer et al. [28], Ehlers et al. [14, 15], Deshpande and Fleck [11], Miller [27], as well as one implemented in the finite element software Abaqus [7] and then proceed to validate constitutive formulations implemented in the finite element code `LS-DYNA` [22]. A general review of yield criteria for cellular materials was given in [1].

It contains a classification of several yield criteria according to their dependency (linear or quadratic) on the homogenized mean stress and on the homogenized von Mises equivalent stress. The subject of yielding of anisotropic cellular materials is also treated in considerable detail in this paper. Finally, a very comprehensive review of yield criteria and constitutive models for cellular metals is available in [30].

In the following sections, the most important constitutive models for cellular metals will be presented. This review is restricted to isotropic material behavior, because no complete constitutive model for anisotropic cellular metals was available. With the exception of the GAZT yield criterion (see Sect. 4.3), the derivation of which was found to be interesting with regard to transferring micro-mechanical considerations to the macro-mechanical level, only complete constitutive models including a plastic flow rule are considered.

The yield criteria $F_i(\sigma_\mathrm{e}, p) = 0$ for the presented constitutive models all contain a term quadratic in the hydrostatic pressure p ($= -\sigma_\mathrm{m}$). They can be distinguished further into models for which the von Mises stress σ_e enters F in linear form [18, 27],

$$F_1(\sigma_\mathrm{e}, p) = \frac{\sigma_\mathrm{e}}{a_1} + \frac{p^2}{b_1} - 1 \tag{41}$$

or in quadratic form, with the yield surface being either symmetric about the origin when plotted in the (σ_e, p) plane [4, 11],

$$F_2(\sigma_\mathrm{e}, p) = \frac{\sigma_\mathrm{e}^2}{a_2} + \frac{p^2}{b_2} - 1 \tag{42}$$

or with a center that is offset along the p axis [7, 33],

$$F_3(\sigma_\mathrm{e}, p) = \frac{\sigma_\mathrm{e}^2}{a_3} + \frac{(p - p_0)^2}{b_3} - 1 \tag{43}$$

The yield functions for the constitutive models cited above will be presented in detail in Sects. 4.3 to 4.8. In addition, a more complex yield function which takes into account the third invariant J_3 of the stress deviator tensor [16] will be described in Sect. 4.9.

The constitutive models for cellular metals differ not only in terms of the formulation of their yield function F, but also in terms of their flow potential G. Several models assume associated plastic flow, i.e., $G = F$. Others define a non-associated flow potential, in most cases to allow for an independent calibration of the plastic Poisson's ratio. Lastly, the models differ in terms of the definition of the hardening variable(s) and the corresponding evolution laws. For more details the reader is referred to Sects. 4.4–4.9.

The treatment of the elastic part of the deformation of cellular metals is essentially the same across the constitutive theories presented here. Therefore, the following separate section is dedicated to this subject.

4.2 Linear Elastic Behavior

For the undeformed material, the strain tensor vanishes per definition, i.e., $\varepsilon_{ij} = 0$. Loading the material will induce stresses and strains. If the stress level is small, the deformation may remain purely elastic. Assuming small elastic deformations, the tensor of elastic strains $\boldsymbol{\varepsilon}_{\mathrm{el}}$ can be related to the stress tensor $\boldsymbol{\sigma}$ by a linear relationship of the form

$$\boldsymbol{\sigma} = \mathbb{E}\,\boldsymbol{\varepsilon}_{\mathrm{el}}, \qquad \text{or} \quad \sigma_{ij} = E_{ijkl}\boldsymbol{\varepsilon}_{kl} \tag{44}$$

which is called Hooke's Law. It involves the fourth-order tensor of elasticity $\mathbb{E}$.

For the special case of an isotropic material, only two material parameters λ and μ called the Lamé parameters are necessary for the definition of the tensor of elasticity E_{ijkl}:

$$E_{ijkl} = \lambda\,\delta_{ij}\delta_{kl} + \mu\left(\delta_{ik}\delta_{jl} + \delta_{il}\delta_{jk}\right), \tag{45}$$

The Lamé coefficients λ and μ can be related to the Young's modulus E and the Poisson's ratio ν of the material:

$$\lambda = \frac{E\nu}{(1+\nu)(1-2\nu)}, \quad \mu = \frac{E}{2(1+\nu)} \tag{46}$$

The Young's modulus E relates a uniaxial stress σ to the resulting strain ε in tension direction in a uniaxial tension test: $\sigma = E\varepsilon$.

While the theoretical description of elasto-plastic materials assumes the existence of an elastic deformation regime, it is very difficult to actually observe purely elastic behavior in experiments on cellular metals, especially under compression. The reason is that plastic deformations on the micro-level may appear at very low overall load levels, e.g., at the sample-test machine interface or around microstructural imperfections, even though these stresses are well below the limit or plateau stress of the materials. It is, therefore, often difficult to define a Young's modulus for cellular metals. In order to arrive at a well defined value for E, the unloading modulus is sometimes used, which is typically higher than the apparent modulus at the onset of loading.

The Poisson's ratio ν of an isotropic material is used in the relationship between the longitudinal stress σ_{11} and the transverse strains $\varepsilon_{22} = \varepsilon_{33} = -\nu\sigma_{11}/E$ in a uniaxial tension test. Because of the typically rough surfaces of cellular materials, it is very hard to measure the Poisson's ratio experimentally.

Another important elastic quantity is the shear modulus G, which relates the shear stress τ to the shear angle γ by $\tau = G\gamma$ in a shear test, and is defined as:

$$G = \frac{E}{2(1+\nu)} \tag{47}$$

Finally, the bulk modulus K couples the mean stress σ_{m} to the volumetric strain $\varepsilon_{\mathrm{vol}}$ according to $\sigma_{\mathrm{m}} = K\varepsilon_{\mathrm{vol}}$ and is given by

$$K = \frac{E}{3(1-2\nu)} \tag{48}$$

Hooke's law can be written in a very compact and useful form, when the deviatoric and the volumetric parts of the elastic strain tensor are inserted separately:

$$\boldsymbol{\sigma} = 2G\mathbf{e}^{(\mathrm{el})} + K\varepsilon_{\mathrm{vol}}^{(\mathrm{el})}\mathbf{I} \tag{49}$$

which implies for the deviatoric part $\mathbf{s}$ of the stress tensor that

$$\mathbf{s} = 2G\mathbf{e}^{(\mathrm{el})} \tag{50}$$

The elastic strain energy density W for an isotropic, linear elastic material can be specified in terms of the stress and strain tensors by:

$$W = \frac{1}{2}\boldsymbol{\sigma}:\boldsymbol{\varepsilon}^{(\mathrm{el})} = \frac{1}{2}\left[\mathbf{s} + \sigma_{\mathrm{m}}\mathbf{I}\right]:\left[\mathbf{e}^{(\mathrm{el})} + \frac{1}{3}\varepsilon_{\mathrm{vol}}^{(\mathrm{el})}\mathbf{I}\right] = \frac{1}{2}\left(\mathbf{s}:\mathbf{e}^{(\mathrm{el})} + \sigma_{\mathrm{m}}\varepsilon_{\mathrm{vol}}^{(\mathrm{el})}\right) \tag{51}$$

The last step in this equation uses the identity $\mathbf{I}:\mathbf{I} = 3$, as well as the fact that the double contraction of the deviatoric part of a second-order tensor and the second order tensor of unity gives zero, i.e., $\mathbf{s}:\mathbf{I} = \mathbf{I}:\mathbf{s} = 0$, and $\mathbf{e}^{(\mathrm{el})}:\mathbf{I} = \mathbf{I}:\mathbf{e}^{(\mathrm{el})} = 0$, because $\mathrm{tr}\,(\mathbf{s}) = 0$ and $\mathrm{tr}\left(\mathbf{e}^{(\mathrm{el})}\right) = 0$, respectively, compare Eq. (7). The last term in Eq. (51) indicates that σ_{m} and $\varepsilon_{\mathrm{vol}}$ are energetically conjugate. Using Eq. (50) it can be shown that

$$\frac{1}{2}\mathbf{s}:\mathbf{e}^{(\mathrm{el})} = \frac{1}{2}\sigma_{\mathrm{e}}\varepsilon_{\mathrm{e}}^{(\mathrm{el})} \tag{52}$$

which shows that σ_{e} and ε_{e} are also energetically conjugate.

Since the stress tensor $\boldsymbol{\sigma}$ and the strain tensor $\boldsymbol{\varepsilon}$ are directly related by Hooke's law, expressions for the strain energy density W can be derived which depend either only on the stress or only on the strain measures:

$$W = \frac{1}{2\bar{E}}\left(\sigma_{\mathrm{e}}^2 + \beta^2\sigma_{\mathrm{m}}^2\right) \tag{53}$$

and

$$W = \frac{\bar{E}}{2}\left(\left[\varepsilon_{\mathrm{e}}^{(\mathrm{el})}\right]^2 + \frac{1}{\beta^2}\left[\varepsilon_{\mathrm{vol}}^{(\mathrm{el})}\right]^2\right) \tag{54}$$

where two alternative elastic material parameters $\bar{E}$ and β are used:

$$\bar{E} = \frac{3E}{2(1+\nu)} \qquad \beta^2 = \frac{9(1-2\nu)}{2(1+\nu)} \tag{55}$$

Observing this, Chen and Lu [4] introduced a definition of a characteristic stress $\bar{\sigma}$,

$$\bar{\sigma}^2 = \sigma_e^2 + \beta^2 \sigma_m^2 \tag{56}$$

and a characteristic strain $\bar{\varepsilon}$,

$$\bar{\varepsilon}^2 = [\varepsilon_e]^2 + \frac{1}{\beta^2} [\varepsilon_{vol}]^2 \tag{57}$$

and used them in their definition of a constitutive model for metallic foam, see Sect. 4.6. Using (50) it can be shown that

$$W = \frac{1}{2} \bar{\sigma} \bar{\varepsilon},$$

i.e., that $\bar{\sigma}$ and $\bar{\varepsilon}$ are energetically conjugate, and that the relationship $\bar{\sigma} = \bar{E} \bar{\varepsilon}$ holds.

4.3 The Gibson-Ashby-Zhang-Triantafillou (GAZT) Model

An interesting early contribution to the description of the effective mechanical behavior of cellular materials has been made in [18]. Therein, a definition of a macroscopic limit surface is derived using exclusively generic micromechanical considerations and dimensional analysis.

First, a simple cubic unit cell is proposed, in which straight struts meet in vertices and corners at rectangular angles. The model struts have a length of l and a square cross-section with a side length of t. The relative density ρ_{rel}, which is the quotient $\rho_{rel} = \rho^*/\rho_S$ of the effective, homogenized density ρ^* and the density of the solid material ρ_S, can be expressed considering that the volume of a unit cell is $V^* = l^3$ and the volume of the solid phase is $V_S = C_1 l t^2$, with C_1 being a constant of proportionality which is related to the total length of all struts in the unit cell. With $\rho^* = \rho_S V_S / V^*$ the following relationship between the unit cell dimensions and the relative density is obtained:

$$\rho_{rel} = \frac{V_S}{V^*} = C_1 \left(\frac{t}{l} \right)^2 \tag{58}$$

Next, the plastic limit load under uniaxial macroscopic loading along the principal directions will be investigated. The macroscopic stress σ^* causes forces F in the cell struts, which are proportional to the application area, $F = C_2 \sigma^* l^2$, with C_2 being the corresponding constant of proportionality. The maximum bending moment in the struts is proportional to Fl. The plastic limit moment M_{pl} of a strut with a square cross-section is given by $M_{pl} = \sigma_{ys} t^3/4$, with σ_{ys} being the yield stress of the material, which is assumed to behave ideally plastic for this investigation. Once the bending moments M reach the plastic limit moment M_{pl}, plastic hinges start to form, and the cellular structure collapses. The corresponding uniaxial limit stress σ_{pl}^* can be found by solving $M(\sigma_{pl}^*) l = M_{pl}$ for σ_{pl}^*:

$$\sigma_{\mathrm{pl}}^{*} = C_3 \, \frac{t^3}{l^3} \, \sigma_{\mathrm{ys}} = C_3 \, {\rho_{\mathrm{rel}}}^{3/2} \, \sigma_{\mathrm{ys}} \tag{59}$$

Gibson et al. propose a value of $C_3 = 0.3$ for fitting this relationship to experimental data for the uniaxial plateau stress of foams.

Next, Gibson et al. recall that regular hexagonal 2D honeycomb structures under bi-axial loading ($\sigma_1 = \sigma_2$) do not experience bending moments in their cell walls. Instead, only normal section forces act in cell wall direction in these honeycombs. They investigate collapse of a 3D cellular material under hydrostatic loading by extending this finding to the tri-axial case, claiming that a hydrostatic macroscopic stress state will lead to purely axial compression or tension in the cell struts or walls. Ironically, this assumption is not true for their model microstructure, because it disregards the fact that any kind of normal loading on the unit cell produces bending moments in the struts perpendicular to the loading direction. These bending moments cannot be compensated by loads in the other principal directions.

Disregarding the bending stresses completely, axial stresses σ_{ax} can be obtained for the struts of the unit cell under a macroscopic mean stress σ_{m}. The total volume V_{S} of solid material in the unit cell is given by $V_{\mathrm{S}} = l^3 \rho_{\mathrm{rel}}$. This volume is now divided by three for obtaining an approximation of the volume of the group of struts that run into each of the three principal directions. The sum of the cross-sectional areas of these struts is given by $A = (V_{\mathrm{S}}/3)/l$. For hydrostatic stress states, the macroscopic mean stress σ_{m} is acting on each face of the unit cube, resulting in a total normal traction force of $F_{\mathrm{m}} = \sigma_{\mathrm{m}} l^2$. Combining all of the above, the axial stress σ_{ax} for hydrostatic loading can be calculated as

$$\sigma_{\mathrm{ax}} = \frac{F_{\mathrm{m}}}{A} = \frac{\sigma_{\mathrm{m}} l^2}{(l^3 \rho_{\mathrm{rel}}/3)/l} = \frac{3\sigma_{\mathrm{m}}}{\rho_{\mathrm{rel}}} \tag{60}$$

Plastic collapse under hydrostatic loading occurs when $\sigma_{\mathrm{ax}} = \sigma_{\mathrm{ys}}$.

If the hydrostatic part of any macroscopic stress tensor is assumed to produce only normal stresses in the struts (or the cell walls) then the deviatoric stresses are expected to produce bending moments. Consequently, Gibson et al. describe the relationship between the von Mises stress σ_{e} and the average bending moment M in the struts as

$$M \propto l^3 \sigma_{\mathrm{e}} = l^3 \sqrt{\frac{1}{2} \left[(\sigma_1 - \sigma_2)^2 + (\sigma_2 - \sigma_3)^2 + (\sigma_3 - \sigma_1)^2 \right]} \tag{61}$$

The factor l^3 is based on the fact that traction forces $F \propto \sigma^* l^2$ and bending moments $M \propto Fl$.

For pure bending, the plastic limit moment of a strut is given by $M_{\mathrm{pl}} = \sigma_{\mathrm{ys}} t^3/4$. Superimposing an axial stress σ_{ax} on the strut reduces the limit moment, as can be seen from the following expression for M_{pl} which can be found after some re-arrangement:

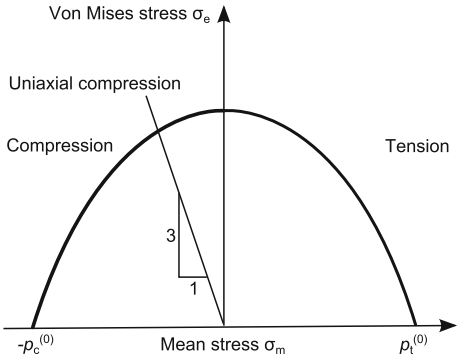

Fig. 10 Sketch of the GAZT yield surface as defined in Eq. (64) and [18]

$$M_{\mathrm{pl}} \propto \sigma_{\mathrm{ys}}\, t^3 \left[1 - \left(\frac{\sigma_{\mathrm{ax}}}{\sigma_{\mathrm{ys}}}\right)^2\right] \tag{62}$$

If the plastic limit moment, which is reduced by the axial stress due to the macroscopic hydrostatic stress according to Eq. (62), is equal to the bending moment induced by the macroscopic deviatoric stress, then the foam will collapse. The corresponding limit condition is found by inserting (60) into (62), considering that $t^3/l^3 = {\rho_{\mathrm{rel}}}^{3/2}$ and some rearranging:

$$\frac{\sigma_{\mathrm{e}}}{\sigma_{\mathrm{ys}}} = \pm\gamma\ {\rho_{\mathrm{rel}}}^{3/2} \left[1 - \left[\frac{3\sigma_{\mathrm{m}}^*}{\sigma_{\mathrm{ys}}\rho_{\mathrm{rel}}}\right]^2\right] \tag{63}$$

The constant γ is a new constant of proportionality, which can be approximated as $\gamma \approx 0.3$ for relevant relative densities ($\rho_{\mathrm{rel}} < 0.3$). The final form of the GAZT limit criterion for the plastic collapse of cellular materials under multiaxial loads is obtained by solving (59) for σ_{ys} using a factor of $C_3 = 0.3$ and inserting the result into (63) with $\gamma = 0.3$:

$$\pm\frac{\sigma_{\mathrm{e}}}{\sigma_{\mathrm{pl}}^*} + 0.81\rho_{\mathrm{rel}}\left(\frac{\sigma_{\mathrm{m}}^*}{\sigma_{\mathrm{pl}}^*}\right)^2 = 1 \tag{64}$$

The dependence on the von Mises stress σ_{e} is linear for this criterion, while the mean stress σ_{m} is squared. Figure 10 shows a generic plot of the yield surface defined by Eq. (64). The parameters $p_{\mathrm{c}}^{(0)}$ and $p_{\mathrm{t}}^{(0)}$ show the compressive and tensile hydrostatic pressures for initial yielding, respectively. Gibson et al. [18] provide similar derivations for failure criteria pertaining to brittle crushing in compression, fracture in tension and elastic buckling. They note, that the corresponding failure surfaces can intersect the failure surface (64) for plastic collapse, and limit the load-carrying capacity of the material further. They also suggest a possible extension of the theory to model failure in anisotropic foams.

4.4 The Miller Model

Miller [27] proposed a constitutive model for cellular materials which is specifically designed for being fitted to the following experimental test results: (a) the compressive and the tensile yield stresses under uniaxial loading conditions, (b) the uniaxial, compressive stress-strain response, and (c) the degree of lateral expansion in a uniaxial compression test.

The corresponding yield function F_{Miller} is an extension of the Drucker-Prager yield function (commonly used for modeling soil) by a term which is a multiple of the square of the hydrostatic pressure p. By adding this term, the plastic Poisson's ratio ν_{pl} can be varied independently of the uniaxial compressive and tensile yield stresses, something, which is not possible with the Drucker-Prager material model. The shape and the size of the yield surface are controlled by three parameters d, γ, and α, as can be seen from the definition of the yield function

$$F_{\text{Miller}} = \underbrace{\underbrace{\sigma_{\text{e}} - d}_{\text{v. Mises}} - \gamma p}_{\text{Drucker}-\text{Prager}} + \frac{\alpha}{d} p^2 \tag{65}$$

Braces in Eq. (65) indicate, which parts of Miller's yield function represent the simpler von Mises yield function for classical metal plasticity and the Drucker-Prager yield function, respectively. Figure 11 shows a sketch of the projection of the Miller yield surface $F_{\text{Miller}} = 0$ onto the von Mises stress versus mean stress plane.

Associated plastic flow is assumed and the increment $d\varepsilon_{ij}^{(\text{pl})}$ of the plastic strain tensor is, therefore, normal to the instantaneous yield surface during active yielding:

$$d\varepsilon_{ij}^{(\text{pl})} = d\lambda \, \frac{\partial F_{\text{Miller}}}{\partial \sigma_{ij}} \tag{66}$$

The definition of the yield function (65) implies, that the yield stresses under uniaxial tension and uniaxial compression differ. Denoting the compressive yield

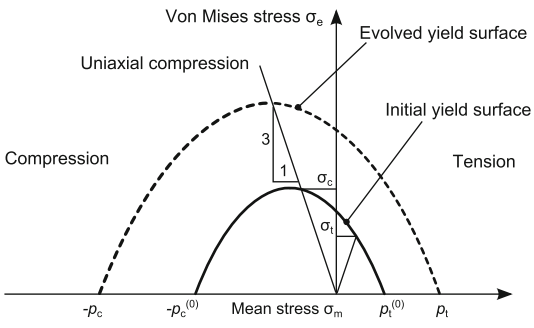

Fig. 11 Sketch of initial and hardened yield surfaces as predicted by the model proposed by Miller [27]

stress as σ_c leads to the definition of the invariants $\sigma_e = \sigma_c$ and $p = \sigma_c/3$, respectively, for uniaxial compression. Inserting these into (65) gives a quadratic equation for σ_c, with the solution[1]

$$\sigma_c = \frac{2d}{1 - \gamma/3 + \sqrt{(1 - \gamma/3)^2 + 4\alpha/9}}, \tag{67}$$

which expresses the compressive uniaxial yield stress σ_c as a function of the yield surface shape parameters. For uniaxial tension, considering that $\sigma_e = \sigma_t$ and $p = -\sigma_t/3$ leads to a similar expression for the uniaxial tensile yield stress:

$$\sigma_t = \frac{2d}{1 + \gamma/3 + \sqrt{(1 + \gamma/3)^2 + 4\alpha/9}} \tag{68}$$

The ratio β between the compressive uniaxial yield stress σ_c and the tensile uniaxial yield stress σ_t follows as

$$\beta = \frac{\sigma_c}{\sigma_t} = \frac{1 + \gamma/3 + \sqrt{(1 + \gamma/3)^2 + 4\alpha/9}}{1 - \gamma/3 + \sqrt{(1 - \gamma/3)^2 + 4\alpha/9}} \tag{69}$$

Since the ratio β can be determined from comparatively simple uniaxial compression and tension tests, it will later be useful for the calibration of the shape parameters of the yield function F_{Miller}.

The next constituent of Miller's material model is the description of the hardening behavior. Miller intends to separate the contribution of hardening of the cell wall material from the hardening which arises from the collapse of cells and the subsequent contact of cell walls. The latter effect is assumed to be a function of the logarithmic volumetric strain ε_{vol}, which relates the volume Δv of an infinitesimal volume element in the deformed configuration to the initial volume ΔV of the same volume element in the undeformed configuration:

$$\varepsilon_{\text{vol}} = \ln \frac{\Delta v}{\Delta V} \tag{70}$$

The stress response of the material in a uniaxial compression test is then described by the uniaxial compressive yield stress σ_c, which is defined as the product of a stress function $\bar{\sigma}_c(\bar{\varepsilon}_{\text{pl}})$, and the dimensionless function $v(\varepsilon_{\text{vol}})$, which depends only on the volumetric strain and is intended to describe the influence of densification:

$$\sigma_c = \bar{\sigma}_c(\bar{\varepsilon}_{\text{pl}})\, v(\varepsilon_{\text{vol}}) \tag{71}$$

[1] For obtaining this original form given in [27], this general relationship is helpful: $a - b = \frac{(a+b)(a-b)}{(a+b)} = \frac{a^2-b^2}{a+b}$.

In [27], $v(\varepsilon_{\mathrm{vol}})$ assumes the value of unity for volumetric strains greater than a volumetric densification strain $\varepsilon_{\mathrm{vol}}^{(\mathrm{D})} (< 0)$. If the volumetric strain falls below the corresponding densification strain, then $v(\varepsilon_{\mathrm{vol}})$ grows rapidly to values much larger than one to model the increase of the stress levels caused by the loss of compliance due to contact of the cell struts or walls.

The function $\bar{\sigma}_{\mathrm{c}}(\bar{\varepsilon}_{\mathrm{pl}})$ depends on the equivalent plastic strain $\bar{\varepsilon}_{\mathrm{pl}}$ and represents the initial mechanical response of the material and the plateau region of the stress-strain relationship. The equivalent plastic strain $\bar{\varepsilon}_{\mathrm{pl}}$ controls the expansion of the yield surface, because it enters Eqs. (71) and (67), respectively, to give the yield function parameter d. The functions $\bar{\sigma}_{\mathrm{c}}(\bar{\varepsilon}_{\mathrm{pl}})$ and $v(\varepsilon_{\mathrm{vol}})$ have to be chosen such that they fit the results of uniaxial compression tests.

To link the expansion of the yield surface under general stress states to the data obtained for the uniaxial case, the concept of accumulated plastic work is used. Herein, the increment of the plastic work given by the product of the increment of the equivalent plastic strain $d\bar{\varepsilon}_{\mathrm{pl}}$ and the instantaneous yield stress σ_{c}, which would correspond to the accumulated plastic strain in a uniaxial compression test, is set equal to the actual increment of the plastic work in the volume element:

$$\sigma_{\mathrm{c}}\, d\bar{\varepsilon}_{\mathrm{pl}} = \sigma_{ij}\, d\varepsilon_{ij}^{(\mathrm{pl})} \tag{72}$$

For the uniaxial compression test it follows that $d\bar{\varepsilon}_{\mathrm{pl}} = d\varepsilon_{11}^{(\mathrm{pl})}$, which is consistent with this definition.

The last item necessary for the calibration of Miller's constitutive theory is the plastic Poisson's ratio ν_{pl}, defined for a uniaxial compression test as the negative ratio of the plastic strains $\varepsilon_{22}^{(\mathrm{pl})}$ in transverse direction and the plastic strains $\varepsilon_{11}^{(\mathrm{pl})}$ in loading direction:

$$\nu_{\mathrm{pl}} = \frac{-\varepsilon_{22}^{(\mathrm{pl})}}{\varepsilon_{11}^{(\mathrm{pl})}} = \frac{\varepsilon_{22}^{(\mathrm{pl})}}{\bar{\varepsilon}_{\mathrm{pl}}} \tag{73}$$

The right part of Eq. (73) follows from the fact that only $\sigma_{11} = -\sigma_{\mathrm{c}} \neq 0$ in the compression test, and, therefore, the definition Eq. (72) of the equivalent plastic strain simplifies to $\sigma_{\mathrm{c}}\bar{\varepsilon}_{\mathrm{pl}} = \sigma_{11}\varepsilon_{11}^{(\mathrm{pl})}$, leading to $\varepsilon_{11}^{(\mathrm{pl})} = -\bar{\varepsilon}_{\mathrm{pl}}$.

The increment of the plastic strain $d\varepsilon_{22}^{(\mathrm{pl})}$ transverse to the loading direction 1 can be found by specializing the flow rule Eq. (66):

$$d\varepsilon_{22}^{(\mathrm{pl})} = d\lambda\, \frac{\partial F_{\mathrm{Miller}}}{\partial \sigma_{22}} \tag{74}$$

The increment of the plastic multiplier $d\lambda$ can be obtained by adapting the implicit definition (72) of the equivalent plastic strain increment $d\bar{\varepsilon}_{\mathrm{pl}}$ to the conditions of uniaxial compression, where only $\sigma_{11} \neq 0$ and, therefore, only $d\varepsilon_{11}^{(\mathrm{pl})}$ contributes to the increment of plastic work:

$$\sigma_c \, d\bar{\varepsilon}_{pl} = \sigma_{11} \, d\varepsilon_{11}^{(pl)} = \sigma_{11} d\lambda \, \frac{\partial F_{Miller}}{\partial \sigma_{11}} \tag{75}$$

Finally, the total plastic strain $\varepsilon_{22}^{(pl)}$ in the transverse direction can be derived from

$$\varepsilon_{22}^{(pl)} = \int_0^{\bar{\varepsilon}_{pl}} \frac{\sigma_c \, d\bar{\varepsilon}_{pl}}{\sigma_{11} \frac{\partial F_{Miller}}{\partial \sigma_{11}}} \frac{\partial F_{Miller}}{\partial \sigma_{22}} \tag{76}$$

For the derivation of the sub-expressions in Eq. (76), partial derivatives of the individual terms of the Miller yield function F_{Miller} are given below:

$$\frac{\partial \sigma_e}{\partial \sigma_{11}} = \frac{1}{2\sigma_e} \left[2\sigma_{11} - \sigma_{22} - \sigma_{33} \right] \tag{77}$$

$$\frac{\partial p}{\partial \sigma_{11}} = -\frac{1}{3} \tag{78}$$

$$\frac{\partial \left(p^2 \right)}{\partial \sigma_{11}} = \frac{2}{9} \left(\sigma_{11} + \sigma_{22} + \sigma_{33} \right) \tag{79}$$

An auxiliary term

$$d_0 = \frac{1}{2} \left(1 - \gamma/3 + \sqrt{(1 - \gamma/3)^2 + 4\alpha/9} \right) \tag{80}$$

is now introduced to stay compatible with Miller. Note, that $\sigma_c = d/d_0$, compare Eq. (67). Inserting Eqs. (77) to (80) into the sub-expressions of Eq. (76) and considering, that for uniaxial compression $\sigma_{11} = -\sigma_c$, $\sigma_{22} = \sigma_{33} = 0$, and $\sigma_e = \sigma_c$ gives the intermediate results

$$\sigma_{11} \frac{\partial F_{Miller}}{\partial \sigma_{11}} = \sigma_c(\bar{\varepsilon}_{pl}, \varepsilon_{vol}) \left(1 - \frac{\gamma}{3} - \frac{2\alpha}{9d_0} \right) \tag{81}$$

$$\frac{\partial F_{Miller}}{\partial \sigma_{22}} = \frac{1}{2} + \frac{\gamma}{3} - \frac{2\alpha}{9d_0} \tag{82}$$

and, finally, an expression for the plastic Poisson's ratio ν_{pl} can be obtained as a function of the yield surface shape parameters:

$$\nu_{pl} = \frac{1/2 + \gamma/3 - 2\alpha/9d_0}{1 - \gamma/3 + 2\alpha/9d_0} \tag{83}$$

The purpose of this operation is to relate the yield surface shape parameters γ and α to the physically more meaningful ratio β between the compressive and the tensile uniaxial yield stresses, Eq. (69), and the plastic Poisson's ratio ν_{pl}:

$$\gamma = \frac{6\beta^2 - 12\beta + 6 + 9(\beta^2 - 1)/(1 + \nu_{\mathrm{pl}})}{2(\beta + 1)^2} \tag{84}$$

$$\alpha = \frac{45 + 24\gamma - 4\gamma^2 + 4\nu_{\mathrm{pl}}(2 + \nu_{\mathrm{pl}})(-9 + 6\gamma - \gamma^2)}{16(1 + \nu_{\mathrm{pl}})^2} \tag{85}$$

Miller implemented the constitutive law for metallic foams described above as a user-defined material subroutine (UMAT) in the commercial finite element code Abaqus. Details of the implementation are not given in [27]. It is important to note that β and ν_{pl}, and, consequently, α and γ are assumed to remain constant during plastic flow for the sake of simplicity. This assumption may not be valid for very large strains. Miller simulated compressive loading of a double notched specimen in plain strain, a Brinell hardness test, and an indentation of foam cores with aluminum face sheets investigating different model materials with varying yield surface parameters. In particular, he examined the influence of the plastic Poisson's ratio ν_{pl}.

A considerable part of the discussion in [27] is devoted to the comparison of the proposed material model to the GAZT model, which can be derived as a special case from the present model by choosing $\gamma = 0$, $\alpha = 0.81\rho_{\mathrm{rel}}$, and $d = \sigma^*_{\mathrm{pl}}$. Miller chose a relative density of $\rho_{\mathrm{rel}} = 0.08$ and obtained a plastic Poisson's ratio $\nu_{\mathrm{pl}} = 0.479$ by means of Eq. (83). Since this value is close to the limit value of $\nu_{\mathrm{pl}} = 0.5$ for plastic incompressibiliy, he concludes that the GAZT material is nearly incompressible in uniaxial compression. This conclusion, however, is only valid under the assumption that the GAZT yield function is coupled with an associative flow rule. This assumption is not supported by the original paper [18] where no mention of the application of an associative flow rule is made.

4.5 The Deshpande-Fleck Foam Models

4.5.1 Introduction

Deshpande and Fleck [11] published data obtained by experiments, which subjected specimens of open and closed-cell metallic foams to axisymmetric compressive stress states, were presented. Based on the experimental findings, two constitutive models were developed, which will be presented in the following sections. The simpler of the two models, the so-called self-similar yield surface model, has influenced the simulation of components made from or containing metallic foams considerably, because it was implemented early in commercial finite element codes such as Abaqus.

The experimental work is equally impressive, because it comprises a method of probing the initial yield surfaces of metallic foams as well as determining the evolution of the yield surfaces under uniaxial and compressive loading. The hardening behavior under uniaxial compression and hydrostatic compression was also investigated. During the uniaxial compression tests, the diameter of the cylindrical

specimens was measured in order to derive the plastic Poisson's ratio, altogether giving a reasonably complete picture of the behavior of the investigated metallic foams under multi-axial loading.

4.5.2 The Self-Similar Yield Surface Model

From their multi-axial compression experiments [11] Deshpande and Fleck concluded, that the investigated foams showed essentially isotropic mechanical behavior, and that the yield surfaces, which they probed with axisymmetric compressive stress states ranging from unixaxial compression to hydrostatic compression, could be approximated well by a yield function F_{DF},

$$F_{\mathrm{DF}} \equiv \hat{\sigma} - Y = 0, \tag{86}$$

where $\hat{\sigma}$ is a suitably defined equivalent stress and Y stands for the uniaxial yield strength. Since isotropic material behavior was considered, the equivalent stress $\hat{\sigma}$ was defined in terms of the von Mises stress σ_{e} and the mean stress σ_{m}:

$$\hat{\sigma} = \sqrt{\frac{1}{1 + (\alpha/3)^2}\left(\sigma_{\mathrm{e}}^2 + \alpha^2 \sigma_{\mathrm{m}}^2\right)} \tag{87}$$

This definition corresponds to an elliptical shape in a von Mises stress versus mean stress diagram, see Fig. 12. The aspect ratio of this ellipse is controlled by the shape parameter α. The limiting case of $\alpha = 0$ corresponds to the von Mises yield criterion, since $\hat{\sigma}$ becomes equal to σ_{e} for this case. Deshpande and Fleck report α values between 1.35 and 2.08 for the foams they investigated.

An associated flow rule was assumed, giving a direction of plastic flow $\dot{\boldsymbol{e}}^{(\mathrm{pl})}$, which is normal to the yield surface:

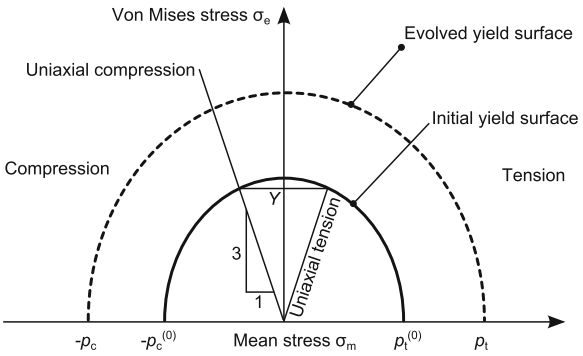

Fig. 12 Sketch of initial and hardened yield surfaces as predicted by the self-similar model proposed by Deshpande and Fleck in [11]

$$\dot{\boldsymbol{\varepsilon}}^{(\mathrm{pl})} = \dot{\lambda}\frac{\partial F_{\mathrm{DF}}}{\partial \boldsymbol{\sigma}} = \dot{\lambda}\frac{\partial \hat{\sigma}}{\partial \boldsymbol{\sigma}} \tag{88}$$

The plastic Poisson's ratio, which is defined as the negative ratio of the transverse logarithmic strain rate $\dot{\varepsilon}_{tt}^{(\mathrm{pl})}$ to the axial logarithmic strain rate $\dot{\varepsilon}_{xx}^{(\mathrm{pl})}$ in a uniaxial compression (or tension) test, can be calculated directly from the flow rule (88), with the help of Table 1 and noting that only $\sigma_{xx} \neq 0$:

$$\nu_{\mathrm{pl}} \equiv -\frac{\dot{\varepsilon}_{tt}^{(\mathrm{pl})}}{\dot{\varepsilon}_{xx}^{(\mathrm{pl})}} = -\frac{(\partial F_{\mathrm{DF}}/\partial \sigma_{tt})}{(\partial F_{\mathrm{DF}}/\partial \sigma_{xx})} = \frac{(1/2) - (\alpha/3)^2}{1 + (\alpha/3)^2} \tag{89}$$

Next, an equivalent strain rate $\dot{\hat{\varepsilon}}$ is introduced, which is the plastic work rate conjugate to the equivalent stress $\hat{\sigma}$:

$$\hat{\sigma}\,\dot{\hat{\varepsilon}} = \sigma_{ij}\dot{\varepsilon}_{ij}^{(\mathrm{pl})} \tag{90}$$

Inserting the flow rule (88) into (90) and solving for $\dot{\hat{\varepsilon}}$ reveals that the rate of this equivalent strain is, in fact, equivalent to the rate of the plastic multiplier $\dot{\lambda}$ in the flow rule (88):

$$\dot{\hat{\varepsilon}} = \underbrace{\frac{\sigma_{ij}}{\hat{\sigma}}\frac{\partial \hat{\sigma}}{\partial \sigma_{ij}}}_{=1}\,\dot{\lambda} = \dot{\lambda} \tag{91}$$

In (91), the application of Euler's theorem (10), which is justified by the fact that $\hat{\sigma}$ is homogeneous of degree one in σ_{ij}, is indicated. Inserting (91) into the plastic flow rule (88) gives

$$\dot{\boldsymbol{\varepsilon}}^{(\mathrm{pl})} = \dot{\hat{\varepsilon}}\frac{\partial F_{\mathrm{DF}}}{\partial \boldsymbol{\sigma}} = \dot{\hat{\varepsilon}}\frac{\partial \hat{\sigma}}{\partial \boldsymbol{\sigma}}. \tag{92}$$

In order to establish a connection between the equivalent plastic strain and the uniaxial yield stress Y, the consistency condition $\dot{F}_{\mathrm{DF}} = 0$ is written using the Jaumann stress rate $\breve{\sigma}_{ij}$:

$$\dot{F}_{\mathrm{DF}} = \frac{\partial F_{\mathrm{DF}}}{\partial \sigma_{ij}}\breve{\sigma}_{ij} + \frac{\partial F_{\mathrm{DF}}}{\partial Y}\dot{Y} = 0 \tag{93}$$

which can be simplified noting that $\partial F_{\mathrm{DF}}/\partial Y = -1$:

$$\dot{Y} = \frac{\partial F_{\mathrm{DF}}}{\partial \sigma_{ij}}\breve{\sigma}_{ij} \tag{94}$$

The hardening modulus H is defined as the ratio of the rate of the equivalent stress to the rate of the equivalent strain:

$$H \equiv \frac{\dot{\hat{\sigma}}}{\dot{\hat{\varepsilon}}} \tag{95}$$

By differentiating F_{DF} with respect to time, the identity $\dot{\hat{\sigma}} = \dot{Y}$ is obtained, which is inserted into Eq. (95) along with the expression for $\dot{Y}$ from (94) to obtain the relationship

$$\dot{\hat{\varepsilon}} = \frac{\dot{\hat{\sigma}}}{H} = \frac{\dot{Y}}{H} = \frac{1}{H}\frac{\partial F_{\mathrm{DF}}}{\partial \sigma_{ij}}\breve{\sigma}_{ij} \tag{96}$$

Finally, the flow rule (92) is rewritten using (96) to obtain the form of Eq. (4) in [11]:

$$\dot{\varepsilon}_{ij}^{(\mathrm{pl})} = \underbrace{\frac{1}{H}\frac{\partial F_{\mathrm{DF}}}{\partial \sigma_{kl}}\breve{\sigma}_{kl}}_{\dot{\lambda}=\dot{\hat{\varepsilon}}}\frac{\partial F_{\mathrm{DF}}}{\partial \sigma_{ij}} \tag{97}$$

Going back to the flow rule (92) and writing out the gradient of the equivalent stress $\partial\hat{\sigma}/\partial\boldsymbol{\sigma}$ gives:

$$\dot{\boldsymbol{\varepsilon}}^{(\mathrm{pl})} = \frac{1}{2\left[1+(\alpha/3)^2\right]}\frac{\dot{\hat{\varepsilon}}}{\hat{\sigma}}\left(3\mathbf{s} + \frac{2}{3}\alpha^2\sigma_{\mathrm{m}}\,\mathbf{I}\right) \tag{98}$$

The stress deviator $\mathbf{s}$ does not contribute to the volumetric plastic strain rate $\dot{\varepsilon}_{\mathrm{m}}$, because $\mathrm{tr}\,(\mathbf{s}) = 0$. Thus, the volumetric plastic strain rate $\dot{\varepsilon}_{\mathrm{m}}$ becomes:

$$\dot{\varepsilon}_{\mathrm{m}} = \mathrm{tr}\left(\dot{\boldsymbol{\varepsilon}}^{(\mathrm{pl})}\right) = \frac{\alpha^2}{1+(\alpha/3)^2}\,\dot{\hat{\varepsilon}}\,\frac{\sigma_{\mathrm{m}}}{\hat{\sigma}} \tag{99}$$

using $\mathrm{tr}\,(\mathbf{I}) = 3$. Inserting (98) into the definition (30) for the effective strain, the effective strain rate can be obtained in the following form:

$$\dot{\varepsilon}_{\mathrm{e}} = \frac{1}{1+(\alpha/3)^2}\,\dot{\hat{\varepsilon}}\,\frac{\sigma_{\mathrm{e}}}{\hat{\sigma}} \tag{100}$$

The equivalent plastic strain rate $\dot{\hat{\varepsilon}}$ can now be formulated in terms of the volumetric and the effective plastic strain rates by expressing σ_{m} in terms of $\dot{\varepsilon}_{\mathrm{m}}$ and $\dot{\hat{\varepsilon}}$ using Eq. (99) and by expressing σ_{e} in terms of $\dot{\varepsilon}_{\mathrm{e}}$ and $\dot{\hat{\varepsilon}}$ based on Eq. (100), followed by inserting the corresponding terms into the definition of the equivalent stress, Eq. (87). Solving the resulting equation for the equivalent strain rate $\dot{\hat{\varepsilon}}$ gives the following expression:

$$\dot{\hat{\varepsilon}}^2 = \left[1+\left(\frac{\alpha}{3}\right)^2\right]\left(\dot{\varepsilon}_{\mathrm{e}}^2 + \frac{1}{\alpha^2}\dot{\varepsilon}_{\mathrm{m}}^2\right), \tag{101}$$

which is useful for calculating the equivalent plastic strain rate $\dot{\hat{\varepsilon}}$ when $\dot{\varepsilon}_{\mathrm{e}}$ and $\dot{\varepsilon}_{\mathrm{m}}$ are known, e.g., from multiaxial experiments. In particular, the equivalent strain rate $\dot{\hat{\varepsilon}}$ enters the definition $H \equiv \dot{\hat{\sigma}}/\dot{\hat{\varepsilon}}$ of the hardening modulus H, as introduced in Eq. (95). The hardening modulus provides the connection between the rate form of the

material law and the experimentally obtained stress-versus-strain data. Specifically, it is required for evaluating the flow rule (97).

Deshpande and Fleck proposed an expression for H which contained a maximum of information from their multi-axial tests. They chose H to depend on the current equivalent strain $\hat{\varepsilon}$ on the one hand and on the direction of the stress path on the other hand. The latter was described by $\eta \equiv |\sigma_\mathrm{m}/\sigma_\mathrm{e}|$ or the ratio $\sigma_\mathrm{e}/\hat{\sigma}$.

The test setup for multi-axial testing consisted of a pressure cell filled with hydraulic fluid and holding a cylindrical foam specimen which was wrapped in insulating layers and further separated from the fluid by a rubber membrane. In this cell the specimen was subjected to a hydrostatic pressure p. In addition, a compressive force acting along the axis of the cylindrical specimen resulted in an additional axial compressive stress σ, bringing the total axial stress to $\sigma_{33} = -(p+\sigma)$. Under these axisymmetric loading conditions, the mean stress becomes $\sigma_\mathrm{m} = -(p+\sigma/3)$, the von Mises stress is equal to $\sigma_\mathrm{e} = |\sigma|$, and the equivalent stress $\hat{\sigma}$ can be calculated easily from Eq. (87).

During the multi-axial experiments, the axial plastic strain $\varepsilon_{33}^{(\mathrm{pl})}$ was measured. This strain can be inserted in Eq. (98) along with σ_m and σ_e, which gives an expression that can be solved for $\hat{\varepsilon}$:

$$\hat{\varepsilon} = \varepsilon_{33}^{(\mathrm{pl})} \frac{\sqrt{\left[1+\alpha^2\eta^2\right]\left[1+(\alpha/3)^2\right]}}{1+\alpha^2\eta/3} \tag{102}$$

The value for α can be found by fitting the yield surface to experimental data or by measuring the plastic Poisson's ratio. For several ratios η between the mean stress and the von Mises stress, the average tangent modulus $\bar{H}$ was then calculated as $\bar{H} = \Delta\hat{\sigma}/\Delta\hat{\varepsilon}$, where $\hat{\varepsilon}$ was a suitable initial increment of the equivalent plastic strain. This operation led to the result that the hardening modulus H can be approximated with reasonable accuracy as a linear function of the direction of the stress path, expressed by the ratio $\sigma_\mathrm{e}/\hat{\sigma}$:

$$H = \left[\frac{\sigma_\mathrm{e}}{\hat{\sigma}} h_\sigma + \left(1 - \frac{\sigma_\mathrm{e}}{\hat{\sigma}}\right) h_p\right] \tag{103}$$

Since the hardening behavior of cellular metals is generally nonlinear, the coefficients h_σ and h_p depend on the instantaneous magnitude of the equivalent strain $\hat{\varepsilon}$. For uniaxial stress states, H becomes equal to h_σ, because $\hat{\sigma} = \sigma_\mathrm{e} = |\sigma_{33}|$. The equivalent strain is equal to the absolute value of the axial plastic strain, $\hat{\varepsilon} = |\varepsilon_{33}^{(\mathrm{pl})}|$. Finally, the coefficient $h_\sigma = h_\sigma(\hat{\varepsilon})$ is equal to the slope of the curve of the Cauchy stress versus the logarithmic plastic strain in loading direction.

The second coefficient h_p can be found from evaluating a hydrostatic compression test in an analogous manner. The equivalent stress for pure hydrostatic loading by a pressure p follows from Eq. (87) by setting $\sigma_\mathrm{e} = 0$:

$$\hat{\sigma}(p) = \frac{\alpha}{\sqrt{1+(\alpha/3)^2}}\, p \tag{104}$$

The rate of the equivalent strain can be found from Eq. (101) as a function of the rate of the logarithmic plastic volumetric strain $\dot{\varepsilon}_\mathrm{m}$ by setting $\dot{\varepsilon}_\mathrm{e} = 0$:

$$\dot{\hat{\varepsilon}} = -\frac{\sqrt{1 + (\alpha/3)^2}}{\alpha}\, \dot{\varepsilon}_\mathrm{m} \tag{105}$$

Finally, the coefficient h_p can be obtained:

$$h_p = \frac{-\alpha^2}{1 + (\alpha/3)^2}\, \frac{\dot{p}}{\dot{\varepsilon}_\mathrm{m}} \tag{106}$$

Deshpande and Fleck determined the coefficients h_σ and h_p from uniaxial compression and hydrostatic compression tests, respectively, for different materials. Then they were able to approximate the evolution of the hardening modulus H for intermediate stress ratios $\sigma_\mathrm{m}/\sigma_\mathrm{e}$, and to obtain the corresponding $\hat{\sigma}(\hat{\varepsilon})$ curves by integration. These were compared to the respective curves from axisymmetric compression tests with the same stress ratios. The agreement was very well for two different densities (8.4 and 16 % relative density, respectively) of Alporas foam, but the equivalent stresses were overestimated for equivalent strains above 0.3 for Duocel foam with 7 % relative density. In all cases, the response under purely hydrostatic compression and uniaxial compression could be fitted to the experimental results to the desired accuracy as part of the calibration process.

The self-similar yield surface model does not allow for a change of the shape of the yield surface and the yield surface remains centered in the $\sigma_\mathrm{m} - \sigma_\mathrm{e}$ plane. Differences in the hardening behavior under uniaxial loading and under hydrostatic loading, however, can be taken into account. A simplified version of this constitutive theory, which has strongly influenced modeling of cellular materials with commercial finite element codes, will be presented in the following sections.

4.5.3 The Simplified Self-Similar Yield Surface Model

For simplifying the calibration of material model input data, Deshpande and Fleck proposed a simplified version of the self-similar yield surface model, for which the hardening response does not depend any more on the behavior under hydrostatic pressure, but can be defined simply on the basis of the response under uniaxial compression and some assumptions regarding the shape of the yield surface.

Specifically, the function (103) for the hardening modulus H simplifies to

$$H(\hat{\varepsilon}) = h_\sigma(\hat{\varepsilon}) \tag{107}$$

This means that the hardening modulus corresponds to the slope of the uniaxial Cauchy stress versus logarithmic plastic strain curve. To fully define the material behavior, a suitable yield surface ellipticity α has to be chosen in addition to $H = H(\hat{\varepsilon})$.

In [11] it was pointed out that measured $\hat{\sigma}(\hat{\varepsilon})$ curves for different stress paths do not collapse into a single curve, as Eq. (107) would suggest. In particular, the hardening under hydrostatic compression loading is visibly more pronounced than the one under uniaxial compressive loading. Nevertheless, the simplified self-similar yield surface model has been implemented in many commercial finite element codes. One of these implementations will be described in the following.

4.5.4 The Abaqus Implementation of the Simplified Self-Similar Yield Surface Model

The simplified self-similar yield surface model developed by Deshpande and Fleck was originally implemented as a user material subroutine in the finite element code Abaqus [7] by Chen [3]. The definitions of the yield function and the equivalent stress were those of Eqs. (86) and (87) respectively.

Later, the material model became part of the standard material library of Abaqus, with the addition of allowing for an independent calibration of the evolution of the yield surface and the plastic Poisson's ratio. Recall, that for the original self-similar Deshpande/Fleck model, the plastic Poisson's ratio ν_{pl} and the yield surface shape parameter α are directly related by Eq. (89), owing to use of an associated flow rule.

In the Abaqus implementation, a non-associated plastic flow rule is introduced to allow for independent calibrations of the shape of the yield surface and the plastic Poisson's ratio. The corresponding flow potential introduces a new parameter β:

$$G_{\mathrm{CF}} = \sqrt{\sigma_{\mathrm{e}}^2 + \beta^2 p^2} \tag{108}$$

With the help of Table 1, the direction of plastic flow can be found:

$$\frac{\partial G_{\mathrm{CF}}}{\partial \boldsymbol{\sigma}} = \frac{1}{2G_{\mathrm{CF}}} \left(3\mathbf{s} - \frac{2}{3}\beta^2 p \mathbf{I} \right) \tag{109}$$

which is sufficient to calculate the plastic Poisson's ratio ν_{pl}:

$$\nu_{\mathrm{pl}} = \frac{1 - (2/9)\beta^2}{2 + (2/9)\beta^2} \tag{110}$$

and, in turns, the parameter β as a function of the plastic Poisson's ratio ν_{pl}:

$$\beta = \frac{3}{\sqrt{2}} \sqrt{\frac{1 - 2\nu_{\mathrm{pl}}}{1 + \nu_{\mathrm{pl}}}} \tag{111}$$

For zero plastic expansion in the transverse direction during uniaxial compression, i.e., $\nu_{\mathrm{pl}} = 0$, a value of $\beta = 3/\sqrt{2} \approx 2.12$ follows immediately. For incompressible

plastic flow, on the other hand, $\nu_{\mathrm{pl}} = 0.5$, $\beta = 0$, and $G_{\mathrm{CF}} = \sigma_{\mathrm{e}}$, which corresponds to the flow rule of classical (von Mises) plasticity.

In accordance with the simplified self-similar yield surface model proposed by Deshpande and Fleck, the hardening of the foam under multi-axial loading is described exclusively by relating the multi-axial strain state to the stress-strain relationship of a uniaxial compression test by means of an equivalent plastic strain $\bar{\varepsilon}^{(\mathrm{pl})}$.

The evolution of the equivalent plastic strain $\bar{\varepsilon}^{(\mathrm{pl})}$ is assumed to be governed by the principle of equivalent plastic work, leading to the relationship

$$\sigma_{\mathrm{c}} \dot{\bar{\varepsilon}}^{(\mathrm{pl})} = \boldsymbol{\sigma} : \dot{\varepsilon}^{(\mathrm{pl})} \tag{112}$$

For uniaxial tension or compression, only the axial plastic strain contributes to the plastic work, and, consequently, the equivalent plastic strain is identical to the axial plastic strain for these loading cases.

Owing to its simplicity and its availability via the finite element code Abaqus this version of the simplified self-similar yield surface model has become quite popular.

4.5.5 The Differential Hardening Model

The experimental evidence collected by Deshpande and Fleck suggested that both the sizes and the shapes of the yield surfaces of isotropic metallic foams change during plastic loading depending on the direction of loading. In the context of their experiments, where a hydrostatic pressure load and an axial load were superimposed, the direction of loading was expressed by the quotient $|\sigma_{\mathrm{m}}/\sigma_{\mathrm{e}}|$.

Correspondingly, they suggested a quadratic yield function F_{DH} of the mean stress σ_{m} and the von Mises stress σ_{e} which separately takes into account the yield strength S under deviatoric loading and the yield strength P under hydrostatic loading:

$$F_{\mathrm{DH}} \equiv \left(\frac{\sigma_{\mathrm{e}}}{S}\right)^2 + \left(\frac{\sigma_{\mathrm{m}}}{P}\right)^2 - 1 \leq 0 \tag{113}$$

Under uniaxial loading, the yield surfaces of the metallic foams investigated in [11] changed predominantly in size, whereas their shapes remained unaffected. Under hydrostatic loading, on the other hand, the yield surfaces were found to become elongated along the hydrostatic axis. Hydrostatic loading affected the deviatoric yield strengths to varying degrees, depending on the material. For Duocel foam, the uniaxial compressive strength remained nearly constant during hydrostatic loading. For Alporas foam, on the other hand, hydrostatic loading consistently led to an increase in deviatoric strength. Uniaxial loading always increased both the deviatoric yield strength and the hydrostatic yield strength. Figure 13 schematically shows an initial yield surface and evolved yield surfaces for two different stress paths. The yield surfaces remain symmetric with respect to the σ_{e} axis, but their aspect ratio can change.

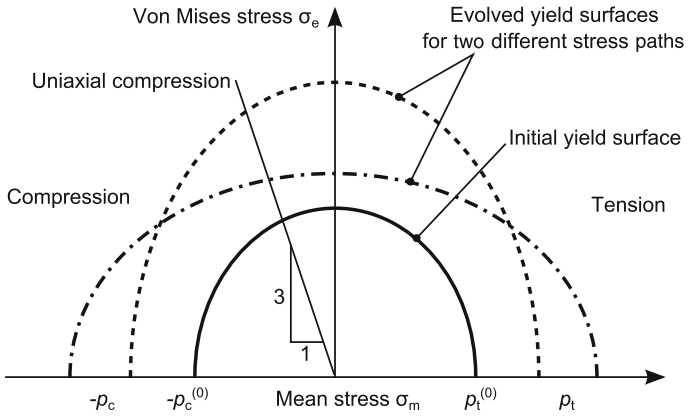

Fig. 13 Sketch of initial and hardened yield surfaces as predicted by the differential hardening model proposed by Deshpande and Fleck [11]

A general hardening rule was thus proposed, which relates the strength values P and S to kinematic quantities ε and γ according to the matrix equation

$$\begin{bmatrix} \dot{P} \\ \dot{S} \end{bmatrix} = \begin{bmatrix} h_{11}\ h_{12} \\ h_{21}\ h_{22} \end{bmatrix} \begin{bmatrix} \dot{\epsilon} \\ \dot{\gamma} \end{bmatrix} \tag{114}$$

The element h_{11} of the hardening matrix relates the rate $\dot{P}$ of the hydrostatic yield stress P to the rate $\dot{\epsilon}$ of a kinematic quantity ϵ, which is connected to the rate $\dot{\varepsilon}_\mathrm{m}$ of the mean strain. The element h_{22} connects the rate of the deviatoric yield strength $\dot{S}$ to the rate $\dot{\gamma}$ in a similar manner. The cross-hardening terms h_{12} and h_{21} connect the hydrostatic strength P and the deviatoric kinematic variable γ as well as the deviatoric strength S and the volumetric straining via ϵ, respectively.

Deshpande and Fleck found good agreement with their experimental data for a choice of the kinematic variables ϵ and γ which makes them plastic work conjugates of P and S, respectively:

$$P\dot{\epsilon} + S\dot{\gamma} = \sigma_\mathrm{e}\dot{\varepsilon}_\mathrm{e} + \sigma_\mathrm{m}\dot{\varepsilon}_\mathrm{m} \equiv \sigma_{ij}\dot{\varepsilon}_{ij}^{(\mathrm{pl})} \tag{115}$$

From this, the following relationships between ϵ and the mean plastic strain ε_m as well as between γ and the effective plastic strain ε_e can be established:

$$\dot{\epsilon} \equiv \frac{\sigma_\mathrm{m}}{P}\dot{\varepsilon}_\mathrm{m} \tag{116}$$

$$\dot{\gamma} \equiv \frac{\sigma_\mathrm{e}}{S}\dot{\varepsilon}_\mathrm{e} \tag{117}$$

In order to tie the coefficients $h_{\alpha\beta}$ of the hardening matrix to experimental results, the flow rule Eq. (97) has to be adapted in a suitable manner:

$$\begin{aligned}\boldsymbol{\varepsilon}^{(\mathrm{pl})} &= \frac{1}{H}\frac{\partial F_{\mathrm{DH}}}{\partial \boldsymbol{\sigma}}\left(\frac{\partial F_{\mathrm{DH}}}{\partial \boldsymbol{\sigma}} : \overset{\circ}{\boldsymbol{\sigma}}\right) \\ &= \frac{1}{H}\left(\frac{3}{S^2}\mathbf{s} + \frac{2}{3}\frac{\sigma_{\mathrm{m}}}{P^2}\mathbf{I}\right)\left[\left(\frac{3}{S^2}\mathbf{s} + \frac{2}{3}\frac{\sigma_{\mathrm{m}}}{P^2}\mathbf{I}\right) : (\dot{\mathbf{s}} + \dot{\sigma}_{\mathrm{m}}\mathbf{I})\right] \\ &= \frac{1}{H}\left(\frac{3}{S^2}\mathbf{s} + \frac{2}{3}\frac{\sigma_{\mathrm{m}}}{P^2}\mathbf{I}\right)\left[\frac{3}{S^2}\mathbf{s}:\dot{\mathbf{s}} + \frac{2}{P^2}\sigma_{\mathrm{m}}\,\dot{\sigma}_{\mathrm{m}}\right] \\ &= \frac{1}{H}\left(\frac{3}{S^2}\mathbf{s} + \frac{2}{3}\frac{\sigma_{\mathrm{m}}}{P^2}\mathbf{I}\right)\left[\frac{2\sigma_{\mathrm{e}}\dot{\sigma}_{\mathrm{e}}}{S^2} + \frac{2\sigma_{\mathrm{m}}\dot{\sigma}_{\mathrm{m}}}{P^2}\right] \end{aligned} \tag{118}$$

The expression in square brackets in Eq. (118) is a scalar multiplier, which can be derived using the relationships $\mathbf{s}:\mathbf{I} = 0$ and $\mathbf{I}:\mathbf{I} = 3$. For the reformulation of the last line of Eq. (118), the identity

$$\dot{\sigma}_{\mathrm{e}} = \frac{3}{2}\frac{\mathbf{s}:\dot{\mathbf{s}}}{\sigma_{\mathrm{e}}} \tag{119}$$

is used. Now, the plastic strain rate tensor $\dot{\boldsymbol{\epsilon}}^{(\mathrm{pl})}$ is split up into a volume-changing part ($\dot{\varepsilon}_{\mathrm{vol}}\mathbf{I}$) and a shape-changing part $\dot{\mathbf{e}}$:

$$(\dot{\varepsilon}_{\mathrm{vol}}\mathbf{I}) = \frac{2}{3}\frac{1}{HP^2}\sigma_{\mathrm{m}}\mathbf{I}\left[\frac{2\sigma_{\mathrm{e}}\dot{\sigma}_{\mathrm{e}}}{S^2} + \frac{2\sigma_{\mathrm{m}}\dot{\sigma}_{\mathrm{m}}}{P^2}\right] \tag{120}$$

$$\dot{\mathbf{e}} = 3\frac{1}{HS^2}\mathbf{s}\left[\frac{2\sigma_{\mathrm{e}}\dot{\sigma}_{\mathrm{e}}}{S^2} + \frac{2\sigma_{\mathrm{m}}\dot{\sigma}_{\mathrm{m}}}{P^2}\right] \tag{121}$$

For each part, the rate of the corresponding scalar quantity $\dot{\varepsilon}_{\mathrm{m}}$ and $\dot{\varepsilon}_{\mathrm{e}}$ (using $\sigma_{\mathrm{e}} = \sqrt{\frac{3}{2}\mathbf{s}:\mathbf{s}}$), respectively, is calculated:

$$\dot{\varepsilon}_{\mathrm{m}} = \dot{\varepsilon}_{\mathrm{vol}}\mathrm{tr}(\mathbf{I}) = \frac{4\sigma_{\mathrm{m}}}{HP^2}\left[\frac{\sigma_{\mathrm{e}}\dot{\sigma}_{\mathrm{e}}}{S^2} + \frac{\sigma_{\mathrm{m}}\dot{\sigma}_{\mathrm{m}}}{P^2}\right] \tag{122}$$

$$\dot{\varepsilon}_{\mathrm{e}} = \sqrt{\frac{2}{3}\dot{\mathbf{e}}:\dot{\mathbf{e}}} = \frac{4\sigma_{\mathrm{e}}}{HS^2}\left[\frac{\sigma_{\mathrm{e}}\dot{\sigma}_{\mathrm{e}}}{S^2} + \frac{\sigma_{\mathrm{m}}\dot{\sigma}_{\mathrm{m}}}{P^2}\right] \tag{123}$$

The hardening modulus H can be eliminated as an unknown by considering the consistency relation as an additional equation:

$$\dot{F}_{\mathrm{DH}} = 0 = \frac{\partial F_{\mathrm{DH}}}{\partial \boldsymbol{\sigma}} : \overset{\circ}{\boldsymbol{\sigma}} + \frac{\partial F_{\mathrm{DH}}}{\partial S}\dot{S} + \frac{\partial F_{\mathrm{DH}}}{\partial P}\dot{P} \tag{124}$$

from which follows, after some rearranging, the hardening modulus H:

$$H \equiv \frac{4\sigma_{\mathrm{m}}^2}{P^3}\left[h_{11}\frac{\sigma_{\mathrm{m}}^2}{P^3} + h_{12}\frac{\sigma_{\mathrm{e}}^2}{S^3}\right] + \frac{4\sigma_{\mathrm{e}}^2}{S^3}\left[h_{21}\frac{\sigma_{\mathrm{m}}^2}{P^3} + h_{22}\frac{\sigma_{\mathrm{e}}^2}{S^3}\right] \tag{125}$$

Now, the hardening coefficients $h_{\alpha\beta}$ can be determined by specializing the expressions (122) and (123) for the mean and the effective strain rates as well as (125) for the hardening modulus H to conform to the loading and deformation conditions of the various experiments. For the hydrostatic compression test, $\sigma_{\mathrm{m}} = -P$ and $\sigma_{\mathrm{e}} = 0$ lead to $h_{11} = \dot{\sigma}_{\mathrm{m}}/\dot{\varepsilon}_{\mathrm{m}}$. At the same time, since $\dot{\gamma} = 0$ for hydrostatic compression of an isotropic material, h_{21} can be expressed as the slope of the deviatoric yield strength versus the plastic volumetric strain curve, $h_{21} = \dot{S}/|\dot{\varepsilon}_{\mathrm{m}}|$, as follows from the second row of the hardening law (114) after setting $\dot{\gamma} = 0$ and applying Eq. (116).

For pure shear loading conditions, $\sigma_{\mathrm{e}} = S$ follows from the yield condition (113) with $\sigma_{\mathrm{m}} = 0$. If the shear loading is characterized by an applied shear stress τ, then $\sigma_{\mathrm{e}} = |\tau|\sqrt{3}$. Thus, the deviatoric yield strength S is related to the shear yield stress τ_{yld} by $S = \tau_{\mathrm{yld}}\sqrt{3}$. Specializing the expression (125) for the hardening modulus for conditions of pure shear and inserting into (123) gives the coefficient $h_{22} = \dot{\sigma}_{\mathrm{e}}/\dot{\varepsilon}_{\mathrm{e}}$. The rate $\dot{\varepsilon}_{\mathrm{e}}$ of the effective strain follows from an engineering shear strain rate $\dot{\gamma}_{12}$ as $\dot{\varepsilon}_{\mathrm{e}} = |\dot{\gamma}_{12}|/\sqrt{3}$. Finally, writing out the first row of the hardening law (114), setting $\dot{\epsilon} = 0$ for pure shear deformation, and applying Eq. (117) gives $h_{12} = \dot{P}/\dot{\varepsilon}_{\mathrm{e}}$.

Deshpande and Fleck also propose a procedure for calibrating the coefficients $h_{\alpha\beta}$ from uniaxial compression tests instead of shear tests. Details can be found in the original paper [11]. Assuming that h_{11} depends only on ϵ, they determined the evolution of this coefficient from the hydrostatic compressive stress versus volumetric compressive strain curve. They found the ratio h_{21}/h_{11} to remain approximately constant and to assume values between 0.4 and 0.55 for the investigated materials. Furthermore, no significant cross-hardening between deviatoric straining $\dot{\gamma}$ and hydrostatic strength $\dot{P}$ was observed, i.e., $h_{12} = 0$. Finally, h_{22} was determined indirectly from the uniaxial and hydrostatic compressive test results.

The differential hardening model was calibrated from unixial compression and hydrostatic compression test results and subsequently used to predict the material behavior for intermediate proportional loading paths. The correlation to experimental results was slightly better than in the case of the self-similar model (see [11]), especially at higher strain levels, and in particular for a Duocel foam of 7.0% relative density. However, the higher accuracy can perhaps not compensate for the added complexity of this model, as Deshpande and Fleck remark themselves.

4.6 Chen and Lu Metallic Foam Material Model

Chen and Lu proposed a material model for metallic foams, which performed well when compared to the more complicated differential hardening model by Deshpande and Fleck (see Sect. 4.5.5). This model was a part of their phenomenological framework of constitutive modeling for elasto-plastic solids [4], which is based on the

definitions of the characteristic stress $\bar{\sigma}$ in Eq. (56) and the characteristic strain $\bar{\varepsilon}$ in Eq. (57) as they were introduced in connection with isotropic elasticity in Sect. 4.2.

Then a 'stress potential' F_{CL} is introduced, which relates multi-axial stress states to the instantaneous total characteristic strain $\bar{\varepsilon}$:

$$F_{\mathrm{CL}} = \bar{\sigma}^2 + C(\bar{\varepsilon})\sigma_{\mathrm{m}}^2 - Y(\bar{\varepsilon}) = 0 \tag{126}$$

No distinction between elastic and plastic strain components is made by Chen and Lu. Therefore, all strain values mentioned in this section pertain to the total strain. Stresses and strains are connected by an associated flow rule $\dot{\epsilon}_{ij} = \dot{\lambda}\partial F_{\mathrm{CL}}/\partial\sigma_{ij}$ the factor $\dot{\lambda}$ being calculated from the consistency condition $\dot{F}_{\mathrm{CL}} = 0$.

The expressions for $\bar{\sigma}$ and $\bar{\varepsilon}$ simplify for some standard experimental settings. For a hydrostatic test with an applied hydrostatic stress of σ_{h} resulting in a volumetric strain of ε_{h}, one gets

$$\bar{\sigma} = \beta|\sigma_{\mathrm{h}}|, \qquad \bar{\varepsilon} = \frac{|\varepsilon_{\mathrm{h}}|}{\beta}, \tag{127}$$

with β as defined earlier in Eq. (55). For a strain ε_{u} caused by a uniaxial stress σ_{u}, the characteristic stress and strain measures become

$$\bar{\sigma} = \frac{\sqrt{9+\beta^2}}{3}|\sigma_{\mathrm{u}}|, \qquad \bar{\varepsilon} = \frac{3}{\sqrt{9+\beta^2}}|\varepsilon_{\mathrm{u}}|, \tag{128}$$

and, finally, for a shear stress τ inducing a engineering shear angle γ:

$$\bar{\sigma} = |\tau|\sqrt{3}, \qquad \bar{\varepsilon} = |\gamma|/\sqrt{3}. \tag{129}$$

The functions $C(\bar{\varepsilon})$ and $Y(\bar{\varepsilon})$ can be determined based on the available experimental results. For example, a characteristic stress-strain curve from a uniaxial compression test with a compressive applied stress of $\bar{\sigma}_{\mathrm{uc}}$ can be used in combination with a corresponding curve obtained in a hydrostatic compression test with an applied compressive hydrostatic stress of $\bar{\sigma}_{\mathrm{hc}}$. Noting that $|\sigma_{\mathrm{m}}| = \bar{\sigma}_{\mathrm{uc}}/\sqrt{9+\beta^2}$ in uniaxial compression and $|\sigma_{\mathrm{m}}| = \bar{\sigma}_{\mathrm{hc}}/\beta$ for hydrostatic compression, the following functions can be obtained after inserting the $\bar{\sigma}$ and σ_{m} values for the two experiments into the yield condition (126):

$$C(\bar{\varepsilon}) = \frac{\bar{\sigma}_{\mathrm{hc}}^2 - \bar{\sigma}_{\mathrm{uc}}^2}{\bar{\sigma}_{\mathrm{uc}}^2/(9+\beta^2) - \bar{\sigma}_{\mathrm{hc}}^2/\beta^2} \tag{130}$$

$$Y(\bar{\varepsilon}) = \bar{\sigma}_{\mathrm{hc}}^2\bar{\sigma}_{\mathrm{uc}}^2\frac{1/(9+\beta^2) - 1/\beta^2}{\bar{\sigma}_{\mathrm{uc}}^2/(9+\beta^2) - \bar{\sigma}_{\mathrm{hc}}^2/\beta^2} \tag{131}$$

For each level of equivalent strain $\bar{\varepsilon}$ the corresponding equivalent stress values $\bar{\sigma}_{\mathrm{uc}}$ and $\bar{\sigma}_{\mathrm{hc}}$ have to be entered in Eqs. (130) and (131) in order to get meaningful functions $C(\bar{\varepsilon})$ and $Y(\bar{\varepsilon})$.

Chen and Lu used these results to fit their functions C and Y to the experimental test results of Deshpande and Fleck [11]. They found that they could predict an intermediate stress versus strain path, which was not used in the calibration process, with the same accuracy as the one possible with the differential hardening model of Deshpande and Fleck [11], even though the calibration process is more simple for their model.

The constitutive equations of Chen and Lu are intended for predicting the multiaxial mechanical response of metallic foams in the compressive regime. Tension or elastic unloading are treated only rudimentarily. The missing separation of elastic and plastic strain contributions falls outside of the framework of classical plasticity theory. Nevertheless, the form of the stress potential F_{CL} and the definitions of the characteristic stress $\bar{\sigma}$ and the characteristic strain $\bar{\varepsilon}$ can inspire other constitutive approaches.

4.7 The Model by Zhang et al.

Even though it was originally developed for polymeric foam materials, the constitutive model proposed by Zhang et al. [33] deserves mention, because it combines a few interesting features which are similar to those already mentioned in previous chapters, and may have actually been providing the motivation for them.

The yield surface is defined in terms of squares of the hydrostatic pressure p and the von Mises equivalent stress σ_{e} and represents a half-ellipse when it is projected onto the p-σ_{e} plane (see Fig. 14):

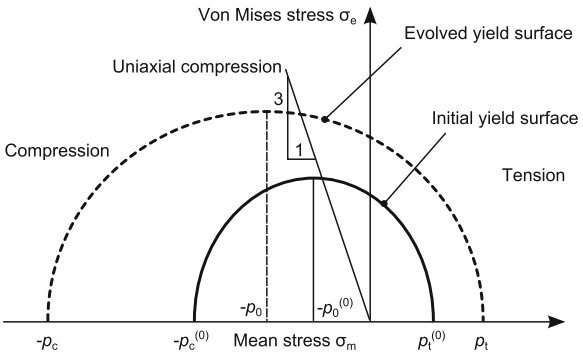

Fig. 14 Sketch of initial and hardened yield surfaces as predicted by the constitutive model proposed in [33]

$$F_{\text{Zhang}} = \frac{\left[p - p_0\right]^2}{a} + \frac{\sigma_e^2}{b} - 1 = 0 \tag{132}$$

The variable p_0 marks the center of the elliptical projection of the yield surface in the p-σ_e plane, compare Fig. 14. The variables a and b define the size and the shape of the yield surface, which are both allowed to change during the plastic deformation process. The terms $p_0(\varepsilon_{\text{vol}}^{(\text{pl})})$, $a(\varepsilon_{\text{vol}}^{(\text{pl})})$, and $b(\varepsilon_{\text{vol}}^{(\text{pl})})$ are all functions of the volumetric plastic strain $\varepsilon_{\text{vol}}^{(\text{pl})}$, i.e., volumetric hardening is assumed. This has the important consequence that the material's response during a shear deformation is perfectly plastic because no volumetric strain hardening occurs.

The present yield surface definition is quite similar to the one of the Abaqus crushable foam model, compare Eq. (135) in Sect. 4.8, but offers more degrees of freedom, because the tensile hydrostatic yield strength is unconstrained.

A non-associated flow rule equivalent to the one in the Abaqus implementation of the Deshpande and Fleck model, see Sect. 4.5.4, is part of the Zhang et al. model. The flow potential has the form

$$G_{\text{Zhang}} = \sqrt{\sigma_e^2 + \alpha p^2} \tag{133}$$

which is almost the same as the one in Eq. (108) with the exception that the constant α corresponds to β^2 in Eq. (108). Following the derivations in Sect. 4.5.4 the parameter α can be related to the plastic Poisson's ratio ν_{pl} via

$$\nu_{\text{pl}} = \frac{9 - 2\alpha}{2(9 + \alpha)} \quad \text{and} \quad \alpha = \frac{9(1 - 2\nu_{\text{pl}})}{2(1 + \nu_{\text{pl}})} \tag{134}$$

and the plastic Poisson's ratio can thus be set independently of other material parameters.

Zhang et al. [33] covers additional interesting aspects of constitutive modeling of polymeric foam materials, namely the numerical implementation of the material model in an explicit finite element code, as well as the mathematical description of the strain-rate sensitivity and and the temperature dependency of the material behavior.

4.8 The Abaqus Crushable Foam Model

The crushable foam model described in this section is a part of the standard material library of the commercial Finite Element Code Abaqus [7]. It became available for the modeling of cellular materials relatively early, at least compared to the other constitutive theories presented here. The crushable foam model was originally developed for PU foams, but an application and calibration of this model for metallic foams is possible, see, e.g., [29]. The model has the following characteristic features:

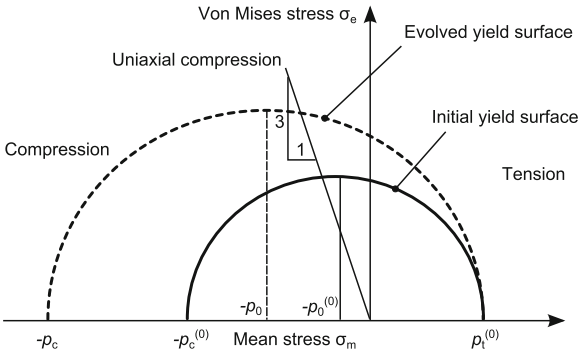

Fig. 15 Sketch of initial and hardened yield surfaces as predicted by the Abaqus crushable foam model [7]. The yield stress $p_t^{(0)}$ for tensile hydrostatic loading and the aspect ratio of the ellipse remain constant

- a constant yield stress value $-p_t^{(0)}$ for hydrostatic tension,
- a non-associated flow rule corresponding to a plastic Poisson's ratio of zero, and
- hardening, which is driven by the compressive volumetric plastic strain $-\varepsilon_{\text{vol}}^{(\text{pl})}$.

The yield surface of the crushable foam material law is defined implicitly by

$$F_{\text{CF}}(\sigma_{\text{e}}, p) = \sqrt{(\sigma_{\text{e}})^2 + \alpha^2 (p - p_0)^2} - B = 0 \tag{135}$$

which depends on two stress invariants, namely the von Mises equivalent stress σ_{e} and the hydrostatic pressure $p\ (= -\sigma_{\text{m}})$, indicating that the material behavior is assumed to be isotropic. The yield surface can geometrically be described as a half-ellipse in the σ_{e} versus σ_{m} plane, see Fig. 15.

The vertex of the ellipse on the axis of positive mean stress is defined by the tensile hydrostatic yield stress $p_t^{(0)}$. As a characteristic feature of the crushable foam model, the yield stress $p_t^{(0)}$ is assumed to remain constant, even if the yield surface expands due to hardening. Consequently, this vertex stays fixed on the σ_{m} axis. The hydrostatic yield pressure p_{c} bounds the yield surface on the negative σ_{m} axis. It can evolve from an initial value $p_{\text{c}}^{(0)}$ to greater values due to hardening.

The center of the yield surface corresponds to a pressure of

$$p_0 = \frac{p_{\text{c}} - p_{\text{t}}^{(0)}}{2} \tag{136}$$

The size of the yield surface is determined by the semi-axis length B in Eq. (135), whereas the parameter α controls the shape. While the yield surface is allowed to expand in the direction of positive hydrostatic pressure, the shape is defined to stay self-similar by keeping the parameter α constant. For fitting the shape parameter α to experimental results, two material parameters k and k_t can be determined:

$$k = \frac{\sigma_{\mathrm{c}}^{(0)}}{p_{\mathrm{c}}^{(0)}} \quad \text{and} \quad k_t = \frac{p_{\mathrm{t}}^{(0)}}{p_{\mathrm{c}}^{(0)}}. \tag{137}$$

The shape parameter (aspect ratio) α then follows as:

$$\alpha = \frac{3k}{\sqrt{(3k_t + k)(3 - k)}} \tag{138}$$

The radius B can be calculated by multiplying the half-length of the yield ellipse along the hydrostatic axis with the shape parameter α:

$$B = \alpha \, \frac{p_{\mathrm{c}} + p_{\mathrm{t}}^{(0)}}{2} \tag{139}$$

The fact that the tensile hydrostatic yield stress $-p_{\mathrm{t}}^{(0)}$ is assumed to remain constant throughout the evolution of the yield surface and, therefore, during any plastic deformation process, takes into account that no hardening due to compaction of the cellular structure is possible under hydrostatic tension.

In order to fit the initial yield surface to experimental data, three points on the initial yield surface have to be determined experimentally. The following list gives candidates for these points:

- initial compressive yield stress in uniaxial compression $\sigma_{\mathrm{c}}^{(0)}$,
- initial tensile yield stress in uniaxial tension $\sigma_{\mathrm{t}}^{(0)}$,
- initial yield stress in simple shear $\tau_{\mathrm{y}}^{(0)}$,
- initial yield stress under hydrostatic pressure $p_{\mathrm{c}}^{(0)}$.

Not included in this list is the initial yield stress under hydrostatic tension $p_{\mathrm{t}}^{(0)}$, because it is almost impossible to determine this value experimentally. It can, nevertheless, be calculated from other yield stresses, for example from $\sigma_{\mathrm{c}}^{(0)}$, $\sigma_{\mathrm{t}}^{(0)}$, and $p_{\mathrm{c}}^{(0)}$, which are comparatively easy to find from experiments:

$$p_{\mathrm{t}}^{(0)} = \frac{p_{\mathrm{c}}^{(0)} \sigma_{\mathrm{c}}^{(0)} \sigma_{\mathrm{t}}^{(0)}}{3\, p_{\mathrm{c}}^{(0)} (\sigma_{\mathrm{c}}^{(0)} - \sigma_{\mathrm{t}}^{(0)}) + \sigma_{\mathrm{c}}^{(0)} \sigma_{\mathrm{t}}^{(0)}} \tag{140}$$

According to [7] the yield strength in hydrostatic tension $p_{\mathrm{t}}^{(0)}$ has to be expected to be considerably lower than the inital yield strength in hydrostatic compression $p_{\mathrm{c}}^{(0)}$, resulting in ratios $p_{\mathrm{t}}^{(0)}/p_{\mathrm{c}}^{(0)} = 0.05$ to 0.10.

While the shape of the yield surface remains constant, its size increases with progressing plastic deformation. The hardening behavior is controlled by a plastic strain measure, which, for this model, is equal to the compressive volumetric strain $-\varepsilon_{\mathrm{vol}}^{(\mathrm{pl})}$. The hardening behavior can be extracted from the stress-versus-strain-results of a uniaxial compression test assuming zero plastic Poisson's ratio. In this case, the uniaxial plastic strain is equal to the volumetric plastic strain.

The assumption of vanishing plastic deformation transverse to any given loading direction, expressed by $\nu_{\mathrm{pl}} = 0$, is, indeed, a feature of the crushable foam material model. It is based on experimental observations, which indicate that cellular materials do not tend to deform significantly in the lateral direction when they are tested in a uniaxial compressive test. Preventing plastic flow normal to the loading direction is achieved by choosing an appropriate non-associated flow rule of the form

$$d\boldsymbol{\varepsilon} = d\bar{\varepsilon}^{(\mathrm{pl})} \, \frac{\partial G_{\mathrm{CF}}}{\partial \boldsymbol{\sigma}} \tag{141}$$

containing the increment of the equivalent plastic strain $d\bar{\varepsilon}^{(\mathrm{pl})}$, which will be investigated in more detail below, and the flow potential function G_{CF}, which is defined in terms of the stress tensor invariants σ_{e} and p as:

$$G_{\mathrm{CF}} = \sqrt{(\sigma_{\mathrm{e}})^2 + \frac{9}{2} p^2} \tag{142}$$

It can be shown that this corresponds to the equivalent tensorial form

$$G_{\mathrm{CF}} = \sqrt{\frac{3}{2} \boldsymbol{\sigma} : \boldsymbol{\sigma}} \tag{143}$$

which can be differentiated with respect to the coordinates of the stress tensor to obtain the direction of plastic flow for the crushable foam model:

$$\frac{\partial G_{\mathrm{CF}}}{\partial \boldsymbol{\sigma}} = \frac{3\boldsymbol{\sigma}}{2 G_{\mathrm{CF}}} \tag{144}$$

Equation (144) indicates a direction of plastic flow which is identical to the stress direction for radial paths in stress space. This means, that loading in any principal direction does, per definition, not cause any plastic deformation in the other principal directions.

Finally, the increment of the equivalent plastic strain $d\bar{\varepsilon}^{(\mathrm{pl})}$ follows from Eq. (141) if the scalar product of both sides with the stress tensor is formed:

$$\boldsymbol{\sigma} : d\boldsymbol{\varepsilon}^{(\mathrm{pl})} = \boldsymbol{\sigma} : \left(d\bar{\varepsilon}^{(\mathrm{pl})} \, \frac{\partial G_{\mathrm{CF}}}{\partial \boldsymbol{\sigma}} \right) = d\bar{\varepsilon}^{(\mathrm{pl})} \, \boldsymbol{\sigma} : \frac{3\boldsymbol{\sigma}}{2 G_{\mathrm{CF}}} = d\bar{\varepsilon}^{(\mathrm{pl})} \, G_{\mathrm{CF}} \tag{145}$$

from which the increment of the equivalent plastic strain can be expressed as

$$d\bar{\varepsilon}^{(\mathrm{pl})} = \frac{\boldsymbol{\sigma} : d\boldsymbol{\varepsilon}^{(\mathrm{pl})}}{G_{\mathrm{CF}}} \tag{146}$$

While the definition of the crushable foam yield surface, which relates the stress tensor invariants σ_{e} and p to each other in the form of the equation of an ellipse, is not

unusual for cellular materials, the treatment of the hydrostatic tensile yield strength as being a constant, and the fact that radial loading does not cause any transverse plastic deformation, are unique characteristics of the crushable foam model.

4.9 The Ehlers Model for Cellular Metals

Ehlers and Müllerschön adapted a constitutive model, which was orginally developed for porous and granular porous media, to represent plastic yielding of metal foam [14, 16]. The yield function

$$F_{\text{Ehlers}} = \sqrt{\left[J_2\left(1+\gamma\frac{J_3}{(J_2)^{3/2}}\right)^m + \frac{1}{2}\alpha I_1^2 + \delta^2 I_1^4\right]} + \beta I_1 + \boldsymbol{\varepsilon} I_1^2 - \kappa = 0 \quad (147)$$

depends on the first invariant $I_1 = 3\sigma_{\text{m}} = -3p$ of the stress tensor, the second invariant $J_2 = \frac{1}{2}\mathbf{s}{:}\mathbf{s} = \sigma_{\text{e}}^2/3$ of the stress deviator tensor $\mathbf{s}$ and on the third invariant $J_3 = \det(\mathbf{s})$ of $\mathbf{s}$.

The characteristic which sets apart this material model from the others presented so far is its dependence on the third invariant J_3, which indicates a shape of the yield surface cross-section in the deviatoric plane, which is not circular, but rather triangular with rounded corners. The shape of the deviatoric cross-section is controlled by the parameters γ and m in (147). By setting $\gamma = 0$ the influence of the third deviatoric invariant is eliminated and the rounded triangular shape of the yield surface cross sections in the deviatoric plane changes into a circular shape.

For this material model, a non-associated flow rule is proposed with a plastic flow potential G_{Ehlers}, which is presented here in the form given in [13]:

$$G_{\text{Ehlers}} = \sqrt{\left[\psi_1 J_2 + \frac{1}{2}\alpha I_1^2 + \delta^2 I_1^4\right]} + \psi_2\beta I_1 + \varepsilon I_1^2 \quad (148)$$

In an earlier publication [14] the parameters ψ_i were set to unity, $\psi_1 = \psi_2 = 1$, and the plastic potential is fully defined by the parameters describing the yield surface.

The Ehlers model has the largest number of parameters required for defining the shape of the initial yield surface, namely seven. For hardening along arbitrary strain paths, these parameters may even be history-dependent. This makes material calibration somewhat complicated, as a large number of different tests (uniaxial compression/tension, axial-symmetric compression and biaxial loading in [16]) and a least-square fitting process are required. For an AlSi7Mg foam with an average apparent density of 0.3 g/cm^3 (produced by Hydro Aluminium) the following parameters are given for the initial yield surface in [16]: $\alpha = 0.0196$, $\beta = 0.07$, $\gamma = 1.4$, $\delta = 0.0176\,\text{MPa}^{-1}$, $\boldsymbol{\varepsilon} = 0.00196\,\text{MPa}^{-1}$, $\kappa = 2.02\,\text{MPa}$, $m = 0.61$. Figure 16 shows a rendering of the yield surface in the principal stress space. By projecting the yield surface along the direction of the hydrostatic axis, the non-circular deviatoric

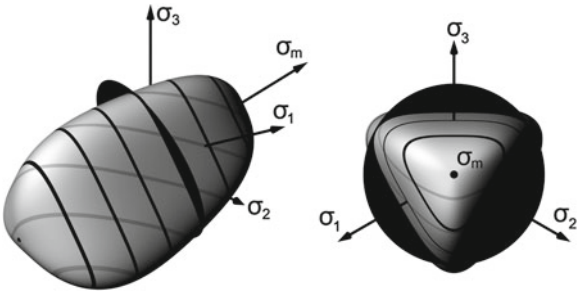

Fig. 16 Rendering of the Ehlers et al. yield surface in principal stress space using material parameters from [16]. The black contour lines indicate levels of constant mean stress in intervals of 1 MPa. The black disc represents the π plane and has a radius corresponding to $\sigma_e = 4.5$ MPa. The grey contour lines indicate cross-sections with constant σ_3

cross-sections can be made clearly visible, see Fig. 16 (right). The quality of the fit of the yield surface(s) to the experimental yield points is illustrated in [12] where both yield surface shapes which deviate from simple ellipsoidal shapes and triangular cross-sections in the deviatoric plane are well documented.

5 Discussion and Conclusions

Existing material laws for metallic foams are adequate for modeling simple deformation histories and predominantly radial stress paths. More complex mechanical processes such as successive perpendicular loading will require more sophisticated modeling techniques to account for the anisotropy caused by changing loading or deformation directions, see Deshpande and Fleck [11] and Hanssen [24].

Perhaps the most restricting feature about the available foam models is the absence of appropriate fracture models. Metal foams are very prone to softening and premature failure under tensile stress states, the overall behavior being governed by progressive failure of the cell walls in this regime. Since fracture is often observed in real-world applications of metal foams, the introduction of corresponding simulation methods is necessary.

A correct calibration of the material parameters based on experimental data is indispensable for the success of any finite element simulation. In most cases, a uniaxial compressive test is the minimum requirement for this calibration. For more sophisticated constitutive models additional data on the yield surface shape and the hardening behavior has to be provided by the user. This requires information about the mechanical behavior of the material under multi-axial loading conditions. Since multi-axial experimental data is scarce the user must rely on appropriate assumptions, which can be derived either from micro-mechanical finite element simulations or via parameter identification techniques (that is, by minimizing the discrepancy between

simulations and experimental results, e.g., a sphere indentation test). The more parameters enter any given constitutive law, the more complicated the calibration process may become. As a consequence, comparatively simple constitutive laws such as the simplified self-similar yield surface model, compare Sect. 4.5.3, see more frequent application, and are often sufficient if the loading conditions are simple enough.

When cellular metals and metallic foams will see more widespread use, and safety-relevant applications such as crash-protection will require more accurate material models, then further advances in the constitutive modeling of cellular metals are to be expected. This contribution hopefully provides the reader with a good starting point for further developments.

Acknowledgments The author would like to thank Lorna J. Gibson, Ronald E. Miller, Vikram S. Deshpande, and Wolfgang Ehlers for helpful discussions regarding their respective publications. The author also wants to thank Maria Steininger for her help with obtaining some of the publications cited in this article.

References

1. Abrate, S.: Criteria for yielding or failure of cellular materials. J. Sandw. Struct. Mat. **10**(1), 5–51 (2008)
2. Bitsche, R.: Space-filling polyhedra as mechanical models for solidified dry foams. Vienna University of Technology, Vienna, Diploma thesis (2005)
3. Chen, C.: Manual for a UMAT user subroutine. Technical Report CUED/C-MICROMECH/TR.4, Department of Engineering, Cambridge University, Cambridge (1998)
4. Chen, C., Lu, T.J.: A phenomenological framework of constitutive modelling for incompressible and compressible elasto-plastic solids. Int. J. Sol. Struct. **37**, 7769–7786 (2000)
5. Combaz, E., Bacciarini, C., Charvet, R., Dufour, W., Dauphin, F., Mortensen, A.: Yield surface of polyurethane and aluminium replicated foam. Acta Mater **58**, 5168–5183 (2010)
6. Combaz, E., Bacciarini, C., Charvet, R., Dufour, W., Mortensen, A.: Multiaxial yield behaviour of Al replicated foam. J. Mech. Phys. Solids **59**, 1777–1793 (2011)
7. Dassault Systèmes (2012) Abaqus 6.12 Theory Manual. Dassault Systèmes Simulia Corp., Providence, Rhode Island.
8. Daxner, T., Denzer, R., Böhm, H.J., Rammerstorfer, F.G., Maier, M.: Simulation des elasto-plastischen Verhaltens von Metallschaum mit Hilfe von 2D und 3D Einheitszellen-Modellen. Mater-wiss u Werkst-techn **31**, 447–450 (2000)
9. Daxner, T., Böhm, H.J., Rammerstorfer, F.G.: Numerical investigation of local yielding in metallic foams. In: Banhart, J., Fleck, N.A., Mortensen, A. (eds.) Cellular Metals: Manufacture, pp. 413–418. Properties, Applications, Verlag MIT, Berlin (2003)
10. Daxner, T., Bitsche, R., Böhm, H.: Space-filling polyhedra as mechanical models for solidified dry foams. Mater. Trans. **47**(9), 2213–2218 (2006)
11. Deshpande, V.S., Fleck, N.A.: Isotropic constitutive models for metallic foams. J. Mech. Phys. Solids **48**, 1253–1283 (2000)
12. Droste, A.: Beschreibung und Anwendung eines elastisch-plastischen Materialmodells mit Schädigung für hochporöse Metallschäume. Ph.D. thesis, University of Stuttgart, Stuttgart (2002)
13. Ehlers, W., Avci, O.: Stress-dependent hardening and failure surfaces of dry sand. Int. J. Numer. Anal. Meth. Geomech. **37**, 787–809 (2013)

14. Ehlers, W., Droste, A.: A continuum model for highly porous aluminium foam. Techn. Mech. **19**(4):341–350 (1999a)
15. Ehlers, W., Droste, A.: FE simulation of metal foams based on the macroscopic approach of the theory of porous media. In: Banhart, J., Ashby, M.F., Fleck, N.A. (eds.) Metal Foams and Porous Metal Structures, pp. 299–302. Verlag MIT, Bremen (1999b)
16. Ehlers, W., Müllerschön, H., Klar, O.: On the behaviour of aluminium foams under uniaxial and multiaxial loading. In: Banhart, J., Ashby, M.F., Fleck, N.A. (eds.) Metal Foams and Porous Metal Structures, pp. 255–262. Verlag MIT, Bremen (1999)
17. Gibson, L.J., Ashby, M.F.: Cellular Solids: Structure and Properties, 2nd edn. Cambridge University Press, Cambridge, New York (1997)
18. Gibson, L.J., Ashby, M.F., Zhang, J., Triantafillou, T.C.: Failure surfaces for cellular materials under multiaxial loads—I. Modelling. Int J Mech Sci **31**(9), 635–663 (1989)
19. Gong, L., Kyriakides, S.: Compressive response of open cell foams. Part II: Initiation and evolution of crushing. Int. J. Sol. Struct. **42**(5–6):1381–1399 (2005)
20. Gong, L., Kyriakides, S., Triantafyllidis, N.: On the stability of Kelvin cell foams under compressive loads. J. Mech. Phys. Solids **53**, 771–794 (2005)
21. Gradinger, R.C.: Das mechanische Verhalten von Aluminiumschaum bei Druck—und Crushbelastung – Experimente und numerische Simulation. Vienna University of Technology, Vienna, Diploma thesis (1997)
22. Hallquist, J.O.: LS DYNA Theoretical Manual. Livermore Software Technology Corporation, Livermore, CA (1998)
23. Hanssen, A.G.: Structural crashworthiness of aluminium foam-based components. Ph.D. thesis, Norges Tekniske Høgskole, Trondheim, Norway (2000)
24. Hanssen, A.G., Hopperstad, O.S., Langseth, M., Ilstad, H.: Validation of constitutive models applicable to aluminium foams. Int. J. Mech. Sci. **44**(2), 359–406 (2002)
25. Laroussi, M., Sab, K., Alaoui, A.: Foam mechanics: nonlinear response of an elastic 3D-periodic microstructure. Int. J. Sol. Struct. **39**(13–14), 3599–3623 (2002)
26. Lubliner, J.: Plasticity Theory. Macmillan Publishing Company, New York (1990)
27. Miller, R.E.: A continuum plasticity model for the constitutive and indentation behaviour of foamed metals. Int. J. Mech. Sci. **42**, 729–754 (2000)
28. Schreyer, H.L., Zuo, Q.H., Maji, A.K.: An anisotropic plasticity model for foams and honeycomb. J. Eng. Mech. ASCE **120**(9), 1913–1930 (1994)
29. Seitzberger, M., Rammerstorfer, F.G., Degischer, H.P., Gradinger, R.: Crushing of axially compressed steel tubes filled with aluminium foam. Acta Mechanica **125**, 93–105 (1997)
30. Shahbeyk, S.: Yield/failure criteria, constitutive models, and crashworthiness applications of metal foams. In: Dukhan, N. (ed.) Metal Foams: Fundamentals and Applications, pp. 131–214. DEStech Publications, Lancaster, Pennsylvania (2013)
31. Shim, V.P.W., Tay, B.Y., Stronge, W.J.: Dynamic crushing of strain-softening cellular structures—a one-dimensional analysis. J. Eng. Mat. Tech. ASME **112**, 398–405 (1990)
32. Todt, M.: Long wave instabilities in periodic structures. Vienna University of Technology, Vienna, Diploma thesis (2008)
33. Zhang, J., Kikuchi, N., Li, V., Yee, A., Nusholtz, G.: Constitutive modeling of polymeric foam material subjected to dynamic crash loading. Int. J. Impact. Eng. **21**(5), 369–386 (1998)